Time-richness and phosphatic microsteinkern accumulation in the Cincinnatian (Katian) Ordovician, USA: an example of polycyclic phosphogenic condensation

Benjamin F. Dattilo[1]*, Rebecca L. Freeman[2], Yvonne Zubovic[3], Carlton E. Brett[4], Amanda Straw[5], Mason Frauhiger[5], Amanda Hartstein[5], and Lincoln Shoemaker[6]

[1]Department of Biology, Indiana University-Purdue University Ft. Wayne, Ft. Wayne, IN, 46805, USA <dattilob@pfw.edu>

[2]Department of Earth and Environmental Sciences, University of Kentucky, Lexington, KY, 40506, USA <rebecca.freeman@uky.edu>

[3]Department of Mathematical Sciences, Purdue University Fort Wayne, Fort Wayne, IN, 46805, USA <zubovic@pfw.edu>

[4]Department of Geology, University of Cincinnati, Cincinnati, OH, 45221, USA <brettce@uc.edu>

[5]Earth, Atmospheric and Planetary Science Program, Department of Physics, Purdue University Fort Wayne, Fort Wayne, IN, 46805, USA <amandastraw16@gmail.com>, <mfrauhiger@gmail.com>, <harter05@pfw.edu>

[6]Department of Geological Sciences, Ball State University, Muncie, IN, 47306, USA <lmshoemaker@bsu.edu>

*Corresponding author

Highlights:

- The PPC bed model explains small shelly fossil-style preservation

- Phosphatic steinkern concentration correlates with textural maturity

- Sediment starvation favors phosphogenesis and phosphatic sediment concentration

- Phosphatic microsteinkern-rich sediments are time-rich shell beds

- Carbonate textural maturity may result from minor stratigraphic condensation

Competing interests: None

Abstract. Millimeter-scale phosphatic steinkern preservation is a feature of the taxonomically enigmatic Early Cambrian "small shelly faunas", but this style of preservation is not unique to the Cambrian; it is ubiquitous, if infrequently reported, from the Phanerozoic record. The polycyclic phosphogenic condensation (PPC) model envisions both the genesis and concentration of phosphatic microsteinkerns as natural outcomes of shell bed genesis through episodic sediment starvation. This model predicts that more reworked and condensed shell bed limestones will contain more phosphatic microsteinkerns, but that even the least reworked limestones may contain some phosphatic particles. We test this model through examination of vertical thin sections densely collected through a 10-meter interval from the classic Cincinnatian (upper Katian, middle Maysvillian North American Stage) upper Fairview Formation, Miamitown Shale, and lower Grant Lake formations at four localities near Cincinnati, Ohio. For each of approximately 50 distinguishable limestone depositional units in each locality, a 2 x 2 cm square was selected for study. Each square was assigned a textural classification (mud content of intergranular space) and a breakage rank (pristine to comminuted). Phosphatic particle distribution was quantified both by visual estimation and by particle counting, with counts ranging from none detected to over 1000 per 4 cm^2. Our analyses show a strong positive relationship between phosphate content and both textural maturity and fragmentation. This positive relationship is consistent with the PPC model and confirms that textural maturity can reflect the degree of condensation as well as depth-related environmental energy. This finding suggests that shell bed processes of repeated deposition and reworking make a significant contribution to the generation and accumulation of phosphatic particles. If local-scale sedimentary processes and conditions can control this accumulation, temporal changes in phosphatic sediment deposition rates may be linked to earth changes more complexly than through changing ocean chemistry on a global scale.

1. Introduction

The "*Cyclora* fauna" of the North American Mohawkian and Cincinnatian Series (Upper Ordovician; Katian) in the Cincinnati Arch region is a diverse assemblage of millimeter-scale fossils representing typical Late Ordovician marine taxa (Vendrasco et al., 2013; Dattilo et al., 2016). This phosphatized assemblage of primarily small fossils is found throughout the approximately 400 m of Katian strata in the North American midcontinent, but not in the Sandbian strata below, and far less commonly in the Silurian strata above. Elements of the *Cyclora* fauna fossils include gastropod and bivalve steinkerns, echinoderm ossicle stereom molds, and less easily identified molds of bivalve hinge teeth, bryozoan zooecia, "worm tubes" and other miscellanea (Dattilo et al., 2016). This typical Cincinnatian fauna is distinctive only for its preservation style as calcium-fluorapatite (CFA, or "phosphatic") steinkerns. This style is indistinguishable from the preservation of many of the Cambrian small shelly faunas (SSFs; e.g. Matthews and Missarzhevsky, 1975). We refer to this CFA molding as small-shelly-fossil-style preservation (SSF-style preservation). SSF-style preservation does not include soft tissue ("Orsten-style" e.g., Dornbos, 2011) preservation.

The focus of most research into SSF-style preservation has been Cambrian SSF occurrences (Creveling et al., 2014 a, b; Pang et al., 2017). The Cambrian prevalence of this style of preservation has been linked to unusual oceanographic conditions during a "phosphatization window" (Porter, 2004; Donoghue et al., 2006; Creveling et al., 2014 a, b) that closed during the Furongian (Porter, 2004), immediately before the onset of events that led to the Great Ordovician Biodiversification Event (GOBE; e.g. Webby et al., 2004; Servais and Harper, 2018; Stigall et al., 2019). However, a range of post-Cambrian occurrences (e.g. Dzik, 1994; Witzke and Heathcote, 1997; Dattilo et al., 2016; Pruss et al., 2018; Freeman et al., this volume) demonstrate that this phenomenon is not uniquely Cambrian.

The Katian marks a global peak in sedimentary phosphate (Cook and McElhinny, 1979) as well as the initial decline of the GOBE biodiversity plateau (Servais and Harper, 2018). Other post-Cambrian

SSF occurrences have been linked to periods of renewed global oceanic anoxia (e.g. Pruss et al. 2018), which in the case of the Katian might be associated with a known sea level maximum, or with the global increase in volcanism that marks this interval (Rasmussen et al., 2019; Stigall et al., this volume). Phosphogenesis also requires iron hydroxides (e.g. Froelich, 1988), potentially supplied by Katian volcanics (e.g. Young et al., 2009), but the abundant iron-rich clays of the Cincinnati Ordovician were sourced from the nearby Taconic Orogen (e.g. Dattilo et al., 2012). If the mechanism of phosphogenesis can be explained by local conditions, then we might further pursue the question as to whether the Ordovician global peak in sedimentary phosphate is linked to local conditions, (e.g. local volcanic terrains providing the necessary iron), or whether the linkage is mediated by changes in global-ocean chemistry induced by volcanic or eustatic changes. Similarly, changes in biodiversity, such as the decline at the end of the GOBE, might be induced by global oceanic conditions, or may simply be the summation of local conditions across the globe, or some combination of the two (e.g. Kozik et al., 2019).

A deeper understanding of the sedimentary and geochemical processes responsible for this SSF-style preservation is essential if any paleoceanographic interpretations based on this taphonomy are to be made. The occurrence of Ordovician SSF-style preservation in thousands of beds in the Cincinnati-area Ordovician provides a unique opportunity to understand the underlying processes that form millimeter scale phosphatic steinkerns. The process sedimentology of Cincinnatian shell beds is well understood (e.g. Jennette and Pryor, 1993; Brett et al., 2008; Dattilo et al., 2008, Dattilo et al., 2012). The taxonomy of Cincinnatian fossils is mature and thorough (e.g. Cummings, 1908; Caster et al., 1955; Pojeta, 1979) and these rocks are well constrained stratigraphically (e.g. Holland, 1993; Holland, 1998; Holland, 2008b; Brett and Algeo, 2001; Brett et al., 2018; Brett et al. this volume).

Study of insoluble residue from hundreds of microsteinkern-bearing limestones from the Cincinnatian (Freeman et al., 2013; Dattilo et al., 2016) led to the observation that microsteinkerns are nearly ubiquitous in Cincinnatian limestones, but are rare in some and abundant in others. This observation, coupled with a deeper understanding of shell bed genesis in these strata (Brett et al., 2008;

Dattilo et al., 2008, Dattilo et al. 2012) led to a hypothesis for microsteinkern phosphogenesis that simultaneously solves the problem of phosphogenic steinkern formation (phosphogenesis; Jahnke et al., 1983; Froelich et al., 1988; Jarvis et al., 1994) and concentration (phosphate deposition; e.g. Föllmi, 1996; Trappe, 1998) of phosphatic steinkerns.

Freeman et al. (this volume) outlined the polycyclic phosphogenic condensation (PPC) process, a model to explain millimeter-scale phosphatic steinkern formation and accumulation that integrates the episodic starvation shell bed (ESSB) model (Brett et al., 2008; Dattilo et al., 2008, 2012) already developed for the Cincinnatian with standard models of phosphogenesis and phosphorite deposition (Baturin, 1971; Mullins and Rasch, 1985; Föllmi, 1990, 1996; Pufahl et al., 2003). The ESSB model proposes that shell bed limestones in heterolithic successions represent periods of siliciclastic sediment starvation and minor stratigraphic condensation, with longer periods of sea-floor exposure to episodic storms and other reworking events. The PPC model explains both the formation of phosphatic microsteinkerns and their concentration as a direct result of episodic reworking events during intervals of offshore sediment starvation.

The ESSB model and the PPC process both predict measurable changes resulting from longer periods of sediment starvation that can be tested when examined together. The process of starvation in the ESSB model suggests that longer periods of seafloor exposure result in sediments being affected by more reworking events, which winnow mud from shell gravels (mud winnowed or bypassed, *sensu* Smosna, 1989). Furthermore, longer periods of condensation with reworking events should result in more shell fragmentation. The PPC process predicts that longer periods of condensation should yield more phosphatic steinkerns, because phosphogenesis is a slow process linked to burial and decay of organic matter as well as release of mineral-bound phosphorus during periods of fluctuating redox conditions. Both of these processes predict accumulation of effects over time during periods of zero or low net siliciclastic deposition; as sediment is exposed to more high-energy events than in areas of higher sedimentation rates, its bioclasts are further fragmented and phosphogenesis is renewed. Thus the

combined prediction of the ESSB model and the PPC model is that limestones, which are more texturally mature and are composed of more fragmented shells should also yield more phosphatic steinkerns, beyond the geometric effects of tighter grain packing as platy shells are comminuted. The present study tests the predicted relationship between textural maturity and phosphate content through comparison of differing shell bed microfacies in thin section samples from a thin stratigraphic interval in the Maysvillian Stage of the Cincinnatian Ordovician.

2. Background

2.1 Carbonates interbedded with shales are not simply tempestites

The episodic starvation shell bed (ESSB) model was developed after the unexpected falsification of the predictions of the tempestite proximality model in the Cincinnati Ordovician (Miller et al., 2001, Holland et al., 2001, Webber, 2002). The tempestite proximality model was developed in the Triassic Muschelkalk (Aigner, 1985), a succession of interbedded shelly limestones and mudstones. This model explains thin carbonate beds as storm deposits analogous to thin storm-transported beds of sand within muddy successions, with shells either concentrated by winnowing from pre-existing mixed fair-weather sediments, or transported into distal muddy areas from shallower parts of the basin. The tempestite proximality model explains shell beds as records of individual storms. Clustered, amalgamated or thicker shell beds could be the result of shallowing, which brought the seafloor above storm wave base, subjecting it to more frequent disturbance. Proximal successions should consist of less shale and cleaner, more amalgamated limestones, while, in more distal sections, limestones should consist of sparse, muddier, and more widely separated shell bed event deposits.

The tempestite proximality model was subsequently applied to the similar mixed-carbonate and shale deposits of the Upper Ordovician in the Cincinnati Arch region (Tobin, 1982; Jennette and Pryor, 1993). These studies emphasized meter-scale cycles, which consisted of alternating mudstone and

limestone-rich phases. The mudstone was interpreted to be deposited under quiet deeper-water conditions, with shallowing leading to progressive storm winnowing of previously deposited sediments. Evidence used to support the storm-winnowing origin of these beds includes: 1) reworked bioclasts with multi-directional geopetal structures and internal matrix that contrasts with external matrix, 2) mud rip-up clasts, 3) hummocky cross stratification (HCS) in fine sediments, and 4) megaripples and cross beds in coarse sediments.

Later, Holland et al. (2001), Miller et al. (2001) and Webber (2002), in an analysis of the ecological patterns of Cincinnatian cycles, found that the limestone-rich phases did not differ significantly in fauna from the shale-rich phases of meter-scale cycles, effectively falsifying the tempestite proximality model (Aigner 1985) as applied to the Cincinnati Ordovician (Tobin, 1982; and Jennette and Pryor 1993). Holland et al. (1998) argued that the primary control on development of shell beds was greater frequency and/or intensity of storms, without necessary changes in water depth.

Brett et al. (2008), and Dattilo et al. (2008, 2012) documented additional inconsistencies between the Cincinnatian stratigraphic record and the tempestite proximality model. These include the following observations: 1) limestone beds merge, become cleaner and more amalgamated in the distal direction of the basin rather than the proximal direction; 2) shales consist of centimeter to decimeter-scale single event deposits, suggesting that the shale-rich intervals are stacks of event deposits, rather than fair-weather accumulations; 3) storm-related channeling below even the thickest shell beds does not exceed a few centimeters, at least an order of magnitude less than that required to winnow a sufficient number of shells from the underlying shale-rich sediments to account for the thickness of the shell bed itself; 4) spatial ecologic patchiness is preserved, a feature inconsistent with long-range shell transport; and, 5) insufficient upramp shelly platform-area shell sources are present to account for the volume and extent of Cincinnatian shell beds through down-ramp transport.

2.2 The Episodic Starvation Shell Bed (ESSB) model

Brett et al. (2008) and Dattilo et al. (2008, 2012) developed the episodic starvation shell bed model based on these inconsistencies and the following additional observations: First, thicker more amalgamated shell beds are frequently associated with an underlying layer of carbonate concretions, which are sometimes reworked into the bed itself (Brett et al., 2003, 2008). This association suggests long-term stability of the sulfate reduction zone beneath a stable seafloor—the same seafloor on which shells are accumulating. Second, thicker more amalgamated beds do not simply show well-worn shells and high levels of fragmentation; rather, shells exhibit varied levels of abrasion and breakage. Some delicate multi-element skeletons are perfectly preserved and were apparently buried alive, others are merely disarticulated, while others are represented by comminuted fragments in the same bed. Third, thicker and more amalgamated beds tend to show more evidence of taphonomic feedback (Kidwell and Jablonski, 1983; Freeman et al. 2013) with more frequent encrustation, and with earlier ecological stages being more poorly preserved.

The ESSB model infers that shales were deposited rapidly as a succession of depositional events, whereas shell beds accumulated much more slowly with multiple episodes of reworking. These shell beds are preferentially thickened and more amalgamated when and where there were prolonged periods of low siliciclastic sedimentation. During these times of sediment starvation, storms and tsunamis continued to rework the seafloor as usual, and longer periods of low sedimentation resulted in the cumulative effects of larger numbers of high energy events during the gradual accumulation of shells. Each phase of shell-bed accumulation ended with the first event deposit of siliciclastic mud thick enough that it was not subsequently removed by later events, beginning the phase of rapid siliciclastic input that smothered the shelly seafloor, protecting it from further reworking, a process called "obrution" (Brett and Baird, 1986; Brett and Seilacher, 1991).

2.3. Time richness

One conclusion of the ESSB model is that the textural maturity of sediments can reflect the degree of condensation or "time-richness". Time richness of a depositional unit is related to the concept

of "time averaging" (Kidwell and Jablonski, 1983; Kidwell, 1986, 1989) of the fossil assemblage contained in that unit; a time-rich bed will contain a more time-averaged assemblage of fossils and other carbonate or diagenetic clasts. This interpretation is an addition to traditionally-held views on textural "maturity". Maturity is usually interpreted as a function of depositional energy (e.g. Folk, 1959), with less mature sediments accumulating in lower-energy, deeper-water or protected shallow water environments and more mature sediments accumulating in higher-energy, shallow-water environments. This interpretation is intuitive, and a constantly high-energy environment will result in more texturally mature sediments, but not all texturally mature sediments can be linked to high-energy environments. However, even if an environment is affected by an occasional high energy event this will not lead to maturation; rather, it is the repeated action of physical and chemical processes that leads to textural maturation.

For example, the Dunham (1962) system classifies carbonate sediment by depositional carbonate texture (see e.g. Flügel 2004), and was influenced by the recognition that the deposition of most carbonates is affected by hydraulic conditions, a key aspect of siliciclastic sediment classification systems (e.g. Grabau, 1904). Thus, the Dunham system provides a series of ordinal categories—mudstone-wackestone-packstone-grainstone—that represent increasing textural maturity associated with decreasing amounts of the fine-grained matrix component of the sediment. In this system, textural maturity is associated with higher energy environments.

However, the majority of heavily reworked (texturally mature) Cincinnatian limestones were probably not deposited in a ***continuously*** high-energy environment. Many of them are associated with siliciclastic sediment starvation (e.g. no terrigenous original mud deposited, rather than deposition of mud followed by winnowing) and experienced high-energy levels only episodically during storms and tsunamis (Brett and Algeo, 2001; Brett et al., 2008; Dattilo et al., 2008, 2012). Indeed, some highly fragmental shell beds actually have micritic muds in grain interstices in shallower water areas indicating an absence of winnowing but also the absence of terrigenous muds.

In the modern siliciclastic environment of the Gulf of Mexico, dissolution rates outpace shell accumulation rates, and shells only accumulate when they spend more time protected within the sediment and only periodically are disturbed by high-energy events (Davies et al., 1989), and even then, the initial rate of destruction and disintegration is likely to be very high (e.g. Tomašových et al., 2014). Continuous high-energy is more likely to result in complete destruction of all but the most recently produced shells rather than the accumulation of a shell bed. Longer exposure on the seafloor and accumulated exposure to an increasing number of high energy events should lead to more shell fragmentation.

2.4. The polycyclic phosphogenic condensation process

The Baturin process (Baturin 1971) is commonly invoked to explain sedimentary phosphate concentrations, but is difficult to apply in the Cincinnati Ordovician. This model explains the accumulation of phosphate in two phases. The first phase, phosphogenesis, is the slow *in situ* precipitation of phosphate in deeper, quieter water environments (the highstand systems tract of sequence stratigraphy, e.g. Catuneanu, 2002). This initial phase is followed by concentration ("phosphate deposition") which results from shallowing and attendant increasing energy and reworking (the lowstand systems tract) to concentrate the previously formed phosphatic particles into a phosphate-rich deposit. Sedimentologically, the model is similar to the tempestite proximality model, and adds only the geochemical process of phosphogenesis. However, the majority of Cincinnatian shell beds have detectible amounts of phosphate in the form of "*Cyclora*" (small gastropod)-rich SSFs, and, if the tempestite proximality model does not explain the deposition of these beds, it also cannot be used to explain the presence of the phosphatic microsteinkerns within them.

More generally, both the tempestite proximality and the Baturin models present a problem with sedimentary dynamics. In the subtidal marine environment, highstand systems tracts are dominated by rapid sedimentation and progradation, whereas lowstand and subsequent transgressive systems tracts are characterized by slowing sedimentation. In the case of higher-frequency cycles in the subtidal environment, the range of sea-level fluctuation is small compared to total water depth, but the modulation

of sediment supply is still effective on a gently-dipping ramp because transgressions and regressions are relatively large. While the transgressive phase presents an opportunity for reworking, highstand, and especially falling stage sediments are deposited too rapidly to accommodate phosphogenesis.

The polycyclic phosphogenic condensation model (Freeman et al., this volume) builds on the episodic starvation shell bed model (Brett et al., 2008; Dattilo et al., 2008, 2012). It combines known processes of authigenic CFA precipitation (e.g. Jahnke et al., 1983; Froelich et al., 1988; Jarvis et al., 1994) with two models of phosphatic sediment deposition and concentration (the "Baturin model"; Baturin, 1971; Mullins and Rasch, 1985; Föllmi, 1990, 1996, and the "Puhfahl Model"; Puhfahl et al., 2003). This integrated model predicts that phosphatic steinkerns form during iterative cycles of changing redox conditions that are related to the cyclical processes of shell bed reworking accompanied by regular burial and decay of organic matter during high energy events (Fig. 1). The model interprets phosphatic steinkern-enriched sediments as the product of numerous cycles of reworking during prolonged times (tens to a few thousands of years) of low sediment accumulation rates, resulting in the destruction of calcareous shells and the concentration of the more durable CFA steinkerns and grains.
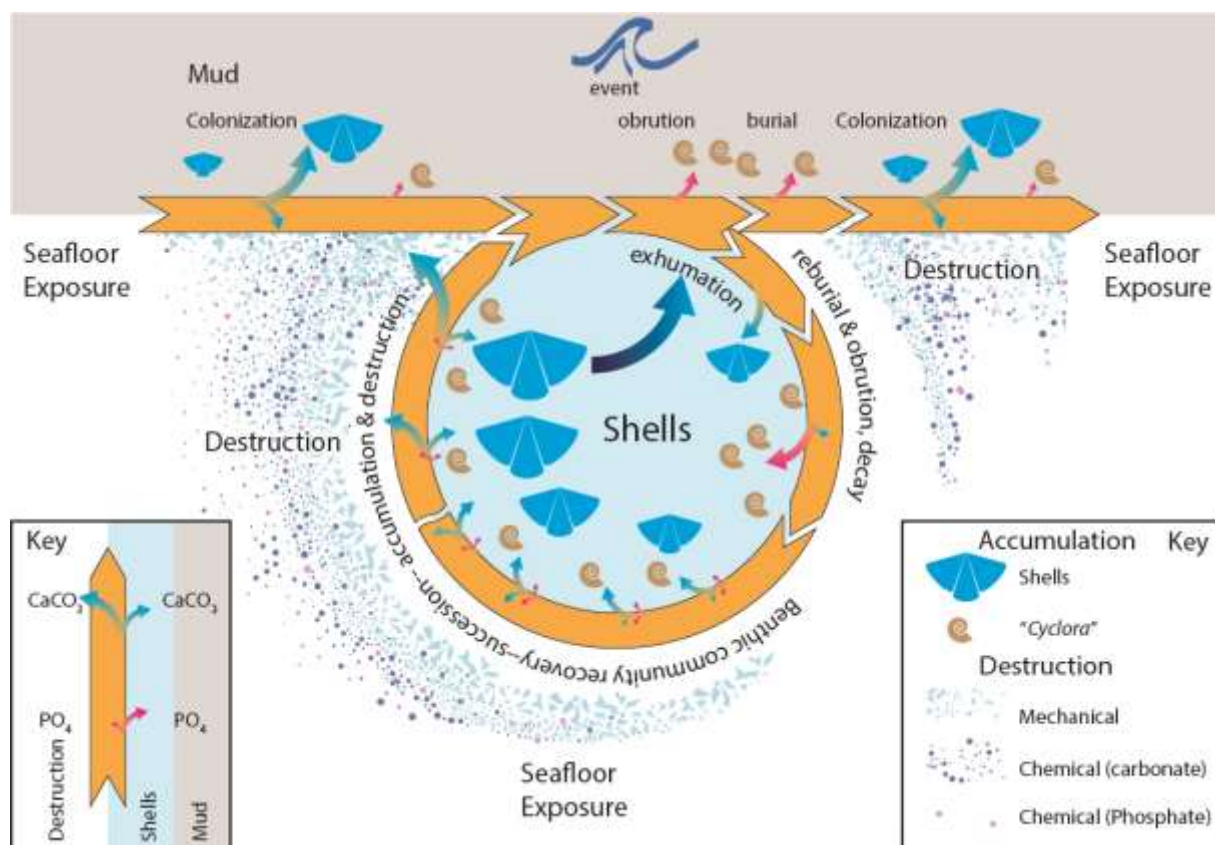
Figure 1.—Diagram of polycyclic phosphogenic condensation (PPC) process in which repeated cycles of disturbance lead to greater and greater concentration of phosphatic microsteinkerns. The gray and blue areas represent burial preservation in mud and shell accumulations respectively. The white area represents loss to fragmentation and dissolution. Blue arrows track the process of shell production and preservation in one direction and the path of shell destruction in the other direction. The pink arrows similarly represent destruction and genesis/preservation of phosphatic particles. The orange arrows represent the progression of time, which may be recorded by progressive influx of mud to make time-poor sediments (straight line), or may cycle back to rework previously deposited sediments resulting in time-rich sediments (circle).

Phosphatic microsteinkerns form diagenetically through authigenic mineral (CFA) precipitation. The proximal source of phosphorus is decaying organic matter ("organic bound"; Creveling et al., 2014b) although under oxic conditions most phosphorus is bound to Fe or Mn oxyhydroxides (e.g. Froelich, 1988), or "iron bound" (Creveling et al., 2014b). This "iron bound" phosphorus is released and becomes available for phosphatic mineral precipitation as conditions in the sediment become more reducing (O'Brien et al., 1990; Lucotte et al., 1994). Thus, the decay of organic matter in the sediment both releases phosphorus directly and, through producing localized decay-induced areas of low oxygen surrounded by redox halos, provides a mechanism for the release of "iron bound" phosphorus as well. As

these reducing areas then shrink and eventually dissipate, and surrounding redox halos collapse, the released phosphorus is swept and concentrated into ever-smaller areas. Phosphatic minerals precipitation is facilitated in a small pore, such as the interior of a small shell, which slows the diffusion of oxygen and allows CFA to precipitate slowly.   Once these authigenic minerals form, they provide a "template" upon which future iterations of phosphatic minerals can nucleate (Föllmi, 1996), in small spaces within the sediments between grains or on minerals that have previously infilled small shell spaces. Only a relatively small amount of phosphorus and resulting phosphatic mineral precipitation is required to produce identifiable phosphatic steinkerns if this authigenic mineral material is primarily cement holding together silt grains.

Shell beds form when sedimentation rates are relatively low (e.g. Kidwell, 1986) and benthic organisms grow in place, with their shells providing a sediment source after their death. Because of the long periods of time required for their formation, shell beds generally show signs of multiple reworking episodes (e.g. Kidwell, 1989). Each episodic high energy event destroys shells and buries living members of the community, resulting in temporary changes in geochemical conditions in the sediment (e.g. Aller, 1982), each time providing an opportunity for further precipitation of phosphate and other authigenic minerals within the sediments. Once phosphatic steinkerns (and intragranular phosphatic infillings) form, this mineral material is more durable than the calcareous shells that comprise much of the surrounding sediments (Lucas and Prévôt, 1991; Schutter, 1996). When a shell bed is exposed for a lengthy period, the accrued result of multiple reworking events is that an equilibrium state may be reached where the rate of shell destruction, through reworking and dissolution (e.g. Powell et al., 2012) as well as ongoing durophagy, bioerosion, and burrowing (e.g. Zuschin et al., 2003) approaches the rate of shell production (Davies et al., 1989) resulting in reduced accumulation rates. As these reworking events proceed, much calcareous shell material is comminuted to fine sediment that is eventually winnowed or dissolved (e.g. Walter and Morse, 1984). Meanwhile, durable phosphatic steinkerns, with a higher specific gravity and durability than calcareous sediments (Föllmi, 1996), continue to form and accumulate, with their

concentration relative to calcareous sediment from broken shells becoming more magnified through each

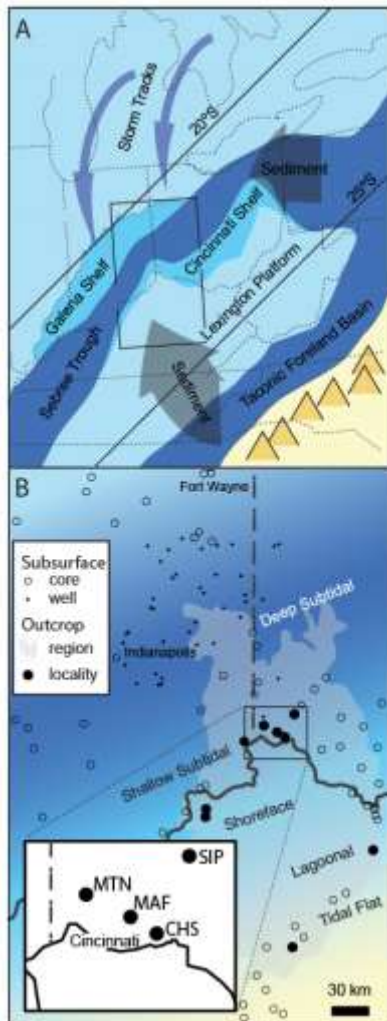cycle of calcareous shell burial and destruction.

Figure 2—Locality Maps. Upper map: paleogeographic setting showing paleo latitudes, sources of sediment influx and inferred storm tracks, the Taconic Orogen (yellow with darker triangular "mountains"), shallow-water platforms (light blue), deeper-water shelves (medium blue), and deepest-water basins (dark blue). Lower map showing outcrop region (shaded), locations of selected outcrop localities (large black circles), subsurface cores (open circles) and logged wells (small black circles) utilized to reconstruct paleo ramp (e.g. Dattilo et al. 2008, 2012). Background colors correspond to labels with yellow-to-blue representing land and peritidal (tidal flat, lagoonal, shoreface) deposits and darker blue representing deeper water (shallow subtidal, deep subtidal). Inset: enlarged area of the Cincinnati region showing the outcrops (largest black circles) from which rock samples were collected from shallow subtidal facies. Localities: CHS, Rice and Gage Street, or Christ Hospital, Cincinnati, Ohio. MAF, Mt Airy Forest, Hamilton County, Ohio cuts along north side of I-74. MTN, roadcuts NW of Miamitown, Ohio around the interchange between I-74 and I-275. And SIP, Sharonville Fossil Park (part of Sharonville Industrial Park), Sharonville, Ohio. Modified from Dattilo et al. (2012).

2.5. Prediction.

The PPC process model suggests that millimeter scale microsteinkerns both form and are

concentrated in place without significant transport during intervals of relative sediment starvation, which

expose the seafloor to multiple reworking events intercalated with recolonization periods. The prediction

is that the concentration of steinkerns will increase with longer residence time of skeletal debris on the

seafloor and with exposure to more reworking events. The ESSB model suggests that shell bed textural maturity is a result of the same condensation. Textural maturity is reflected by, among other things, the Dunham carbonate classification system (Dunham, 1962) and shell fragmentation. Thus, if shell bed textural maturity and phosphate content are both a product of condensation, then shell bed SSF content should increase with increasing textural maturity.
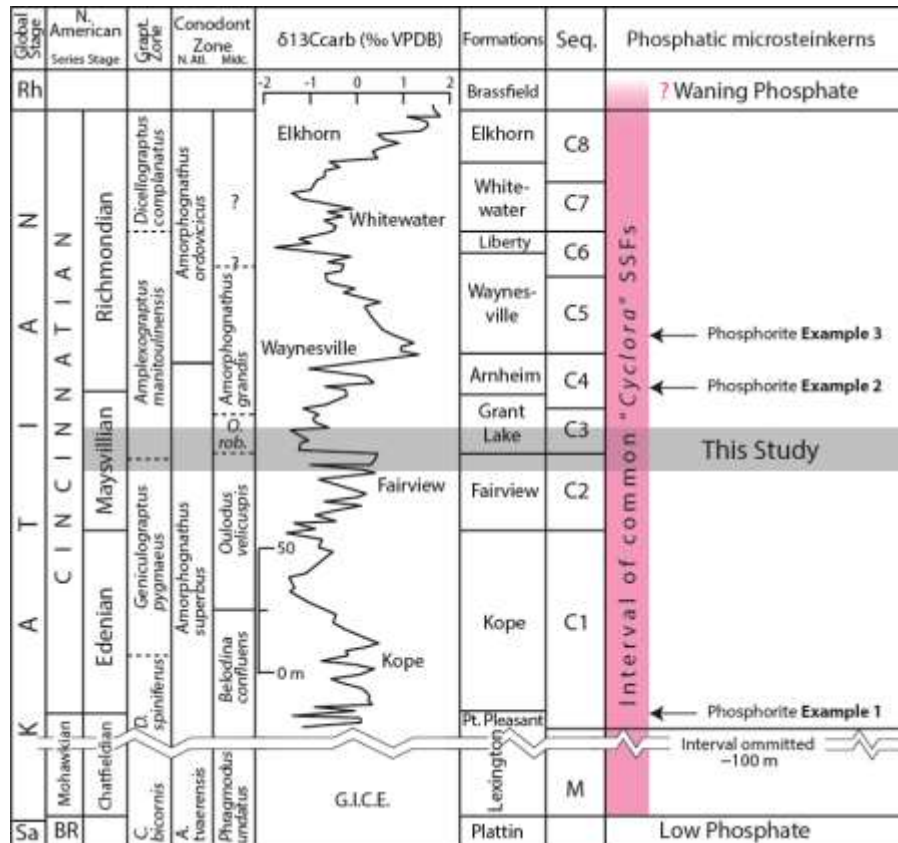

Figure 3.—Stratigraphic context of the study interval. Study shaded gray. Pink shading marks the phosphatic interval of the Katian. Arrows mark the approximate stratigraphic levels for phosphorite examples 1, 2 and 3, which are illustrated in Fig. 4A, B, and C respectively. Cycles are after Holland (1993) and Holland, Patzkowsky (1996, 2007), and Brett et al. (2018; this volume)

3. Materials and methods

3.1. The Cincinnati Ordovician.

Katian strata in the North American midcontinent are composed of alternating shell bed limestones (packstones, wackestones, and grainstones) and siliciclastic mudstones deposited in a cratonic sea at approximately 20–23° South paleolatitude (Mac Niocaill et al., 1997; Jin et al., 2013). Other

authors argue for a more equatorial paleolatitude (Swanson-Hysell and Macdonald, 2017). Depositional environments ranged from peritidal to deep subtidal and most of the beds were deposited in depths above storm wave base (Tobin, 1982; Holland, 1993; Jennette and Pryor, 1993; Holland et al., 1997; Holland, 2008a). Microendoliths and other paleo-depth indicators suggest maximum depths of 60–100 m with most sediments deposited in depths of 30 m or less (Vogel and Brett, 2009; Brett et al., 2015). Siliciclastic sediments are fine grained. Sand is absent, but quartz silt and finer siliciclastics are common and generally well sorted, and originally sourced from the Taconic Orogen. Limestones are much coarser and generally unsorted. The coarsest sorted limestones are beds of laminated calcisiltite, suggesting that currents were not competent enough to transport sand-sized or larger grains.

Storms likely affected vast areas of the shallow seafloor in this subtropical zone (Jennette and Pryor, 1993). The strata preserve widespread soft sediment deformation, interpreted as evidence of earthquake activity, or "seismites" (Ettensohn et al., 2002; McLaughlin and Brett, 2004). Presumably these earthquakes would have produced tsunamis as well.

Cyclora SSFs are found in shell beds throughout the entire ~400 m thickness of the Katian interval in the Cincinnati Region (e.g. Dattilo et al., 2016). Some of these phosphatic deposits are very rich, with phosphatic steinkerns constituting more than half of the rock volume (Fig, 4). We briefly discuss three examples of these rich deposits. The basal Cincinnatian transgressive deposit (Fig. 4A) which is a limestone interval that sits above the unconformity that marks the top of the Lexington Limestone (Brett et al., this volume). This is likely a third order transgressive systems tract deposit. The phosphorite/limestone is about 0.5 m thick, is more phosphatic at the base, with phosphate content decreasing upward to a moderately phosphatic grainstone. The base contains lithoclasts from the underlying low-phosphatic content limestone, and multigenerational, phosphatically cemented clasts of phosphatic steinkerns are common, mixed with single-generation phosphatic steinkerns, and unphosphatized fossils. The middle Cincinnatian Mt. Auburn-Arnheim deposit (Fig. 4B) is thinner and overlies a nodular shale that is devoid of phosphate; its lower contact is a 3rd-order transgressive systems

tract and flooding surface. The upper Cincinnatian Waynesville example (Fig. 4C; e.g. Dattilo et al., 2016) is a 40 cm thick grainstone overlying more than a meter of fossil barren/SSF-free shale and concretionary marl. This bed contains a range of degrees of phosphatization and multigeneration phosphate-cemented clusters of phosphatized fossils. While the succession includes other similarly phosphate-enriched limestones, the majority (thousands of discrete beds) contain some but far fewer (lower concentration of) phosphatic SSFs than shown in these examples, and very few of them mark 3rd /4th or even 5th order stratigraphic surfaces, but are just individual limestone beds.
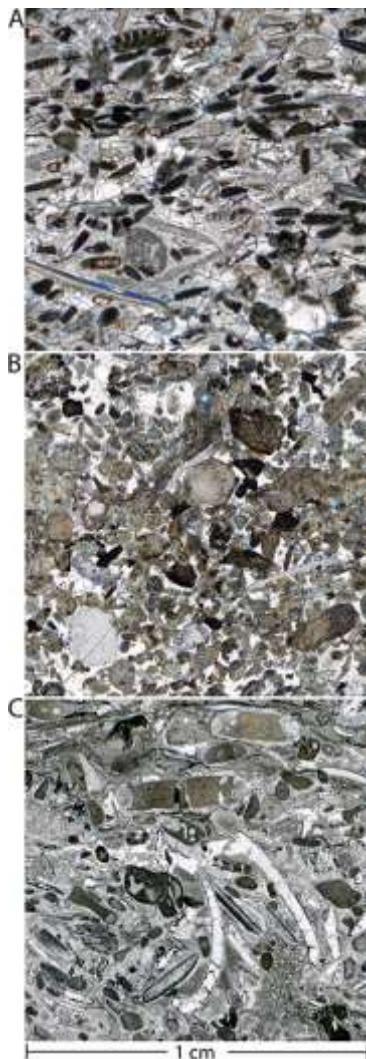

Figure 4.—Thin-section scans (1 cm squares) of three among the more phosphatic limestone beds in the Cincinnati Ordovician. A) the upper Point Pleasant "River Quarry Beds", basal Cincinnatian, at Elkhorn Creek, Kentucky (Fig. 3, Example 1). B) The Arnheim phosphorite bed, Middle Maysvillian, at Madison Indiana (Fig. 3, Example 2). C) Basal transgressive Limestone of the Clarksville Member of the Waynesville Formation (Fig. 3 Example 3).

3.2 The study interval

Of the 400 m of more or less phosphatic Katian sediments, we focus on a 10–12 m interval that contains a number of poorly to moderately phosphatic limestone beds. The interval is in the middle Maysvillian Stage (Katian; Fig. 2; Fig. 3). Rock samples were originally collected as part of an ecological, stratigraphic and stratinomic study (Fig. 2; Dattilo 1996; Dattilo et al. 2008, 2012). The interval includes the upper part of the Fairview Formation, Fairmount Member, the Miamitown Shale Member, and most of the Bellevue Member (Grant Lake Formation; Fig. 3).

Localities (Fig. 2) include Rice and Gage Street, or Christ Hospital (CHS; 39.12073°N, 84.51344°W; Dattilo 1996), Cincinnati, Ohio, Mt Airy Forest, Hamilton County, Ohio cuts along north side of I-74 (MAF; 39.16688°N, 84.57925°W), Roadcuts NW of Miamitown, Ohio around the interchange between I-74 and I-275 (MTN; 39.22122°N, 84.73504°W), and the Trammel Fossil Park (part of Sharonville Industrial Park, SIP; 39.29645°N, 84.40467°W), Sharonville, Ohio. These outcrops span a distance of 22 kilometers from SE to NW (CHS-MAF-MTN) and 21 Kilometers SW to NE (CHS-SIP). Each locality reproduces the same stratigraphic interval comprising 10 to 12 meters of section.

During the period of deposition, paleoslope was just west of north (modern directions) with deeper water to the north, and with sediment input primarily from the current SE. The Miamitown Shale (falling stage C2; Brett et al., 2018; this volume) is regionally truncated beneath the Bellevue contact (sequence boundary of C3; terminology of Brett et al., this volume) and is much thicker in down-ramp sections of Miamitown (5.0 meters; MTN) and Sharonville (4.9 meters; SIP) than it is in the up-ramp section of Cincinnati (1.3 meters; CHS). This interval contains six 5th order cycles that are not treated in the current study.

3.2. Samples and sample treatment

3.2.1. Field collection

The rock samples for this study represent limestone blocks collected at closely but irregularly spaced stratigraphic intervals (~3 to 5 per meter typically, up to 20 per meter at locality CHS; Fig. 5) from the entire 10 to 12 meters measured at each locality in such a way that for most rock samples, a near correlative rock sample (within 0.3 meters) was collected at each of the three other localities. Neither locality nor stratigraphy is considered in this initial analysis— suffice it to say that an irregular spatiotemporal
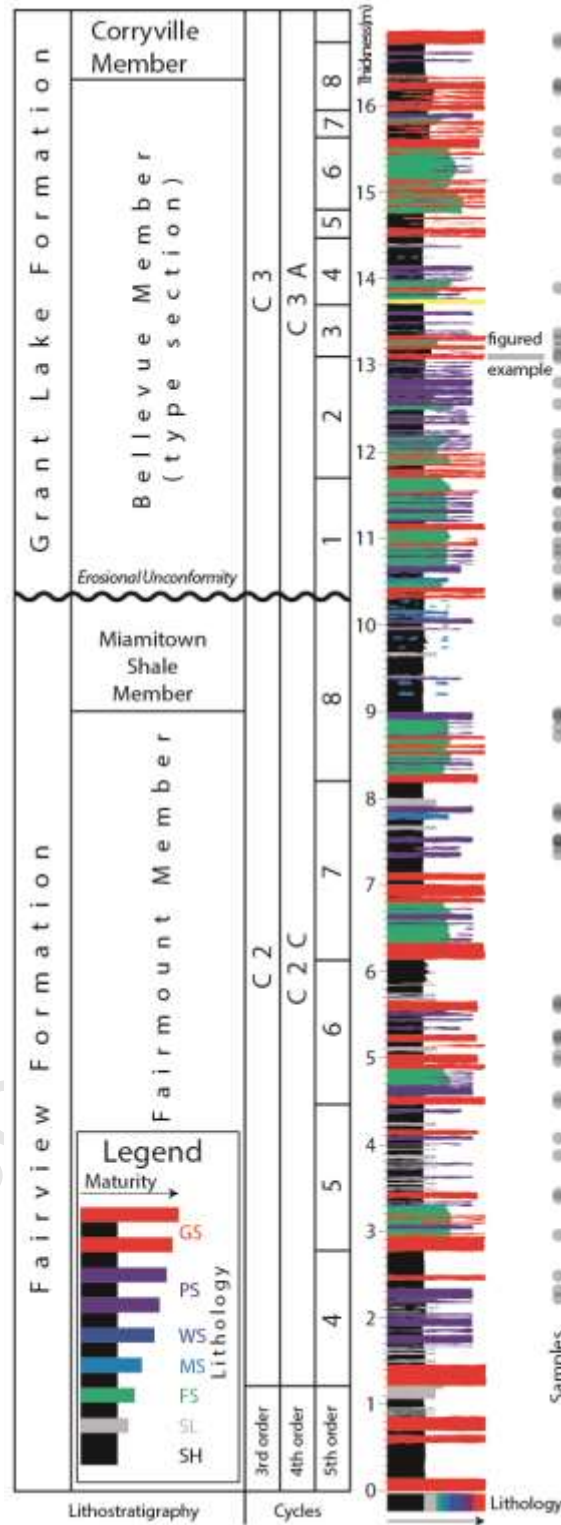

Figure 5.— Stratigraphic column for Christ Hospital (CHS), one of the localities in this study showing the stratigraphic position of thin-section samples (shaded circles) used in this analysis. Lithostratigraphy and cyclic stratigraphy are indicated to the left. Stratigraphic column is coded for carbonate and siliciclastic lithologies by both color and profile. Rectangle "figured example" at 13.1 meters refers to subsequent figure (Fig. 6). Siliciclastics: SH: shale, SL: siltstone, FS: fossiliferous shale. Carbonates, field-determined classification of rudstone matrix: MS: mudstone, WS: wackestone, PS: packstone, GS: grainstone.

grid has been collected (Dattilo, 1996) and processed without consideration for these variables. The

dataset includes a range of microfacies, fragmentation levels, and phosphatic microsteinkern content.
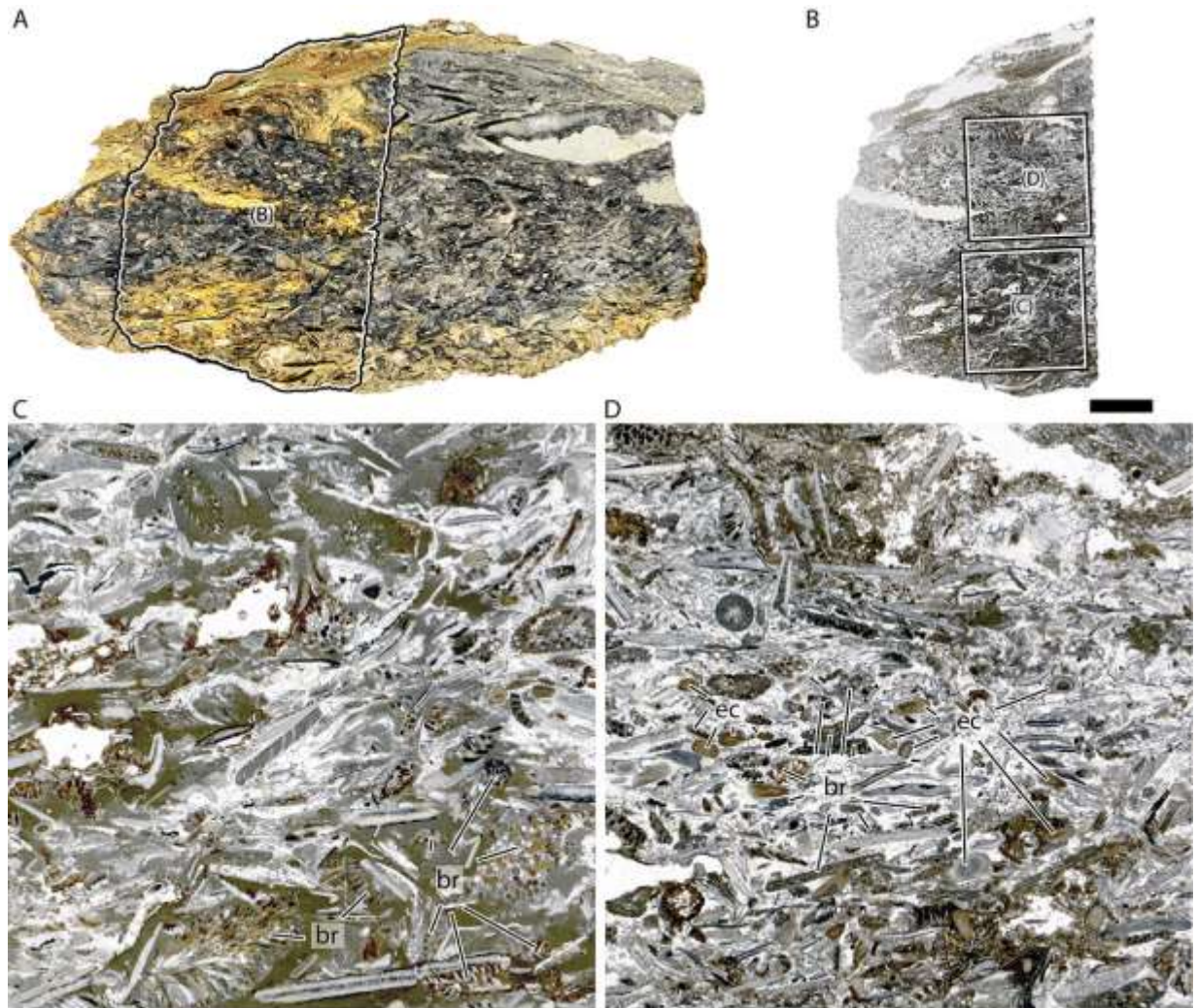
3.2.2. Thin section treatment

Figure 6. Scanned images of rock sample treatments from locality CHS at 13.1 meters (Fig 5). A. Slab surface cut vertically through rock sample and polished, reflected light scan. Outlined area marks the position of the thin section (B, as indicated). Scale bar 1 cm. B. Thin section. Two outlined 2 cm squares are "thin-section sample" (C, D, as indicated) locations. Transmitted light scan. C., D. Two of the 267 thin section-samples (2 cm squares in B; 4 cm^2) on which this study is based, images cropped from the thin-section scan (B). Selected phosphatic fillings of bryozoan zooecia (br) and phosphate-permeated echinoderm ossicles (ec) are marked.

Thin sections were made continuously through the entire stratigraphic interval of each limestone block. The result is that stratigraphically thicker beds are represented by more thin-sectioned area (Fig. 6). Thin sections are made on 75 x 50 mm glass slides. Each thin section was scanned at high resolution on an Epson Perfection V700 photo scanner.

3.2.3. Thin section sampling

Using the scanned thin-section images (Fig. 6), microfacies within depositional units were delineated. A sample area of 4 cm^2 was placed in each microfacies where feasible (if it had a large enough area of uniform lithology), generally as either a 2 cm x 2 cm square or a 1 cm x 4 cm rectangle, or occasionally as a ~1.41 cm x ~2.83 cm area to fit available space. Many limestones in this interval are amalgamated and consist of three or more depositional units, each with one or more distinguishable microfacies and each being a potential sample area, so up to three samples were delineated on each original thin section. In this study, we refer to each of these sampled areas as a "thin-section sample". Given that limestone blocks could result in more than one thin section and that a thin section could have more than one thin-section sample, the resulting number of thin-section samples exceeds the number of original limestone blocks collected, even though not all original blocks (Dattilo, 1996) were incorporated into this study. A total of 267 thin-section samples were used in this study.

3.3. Observational and data gathering techniques
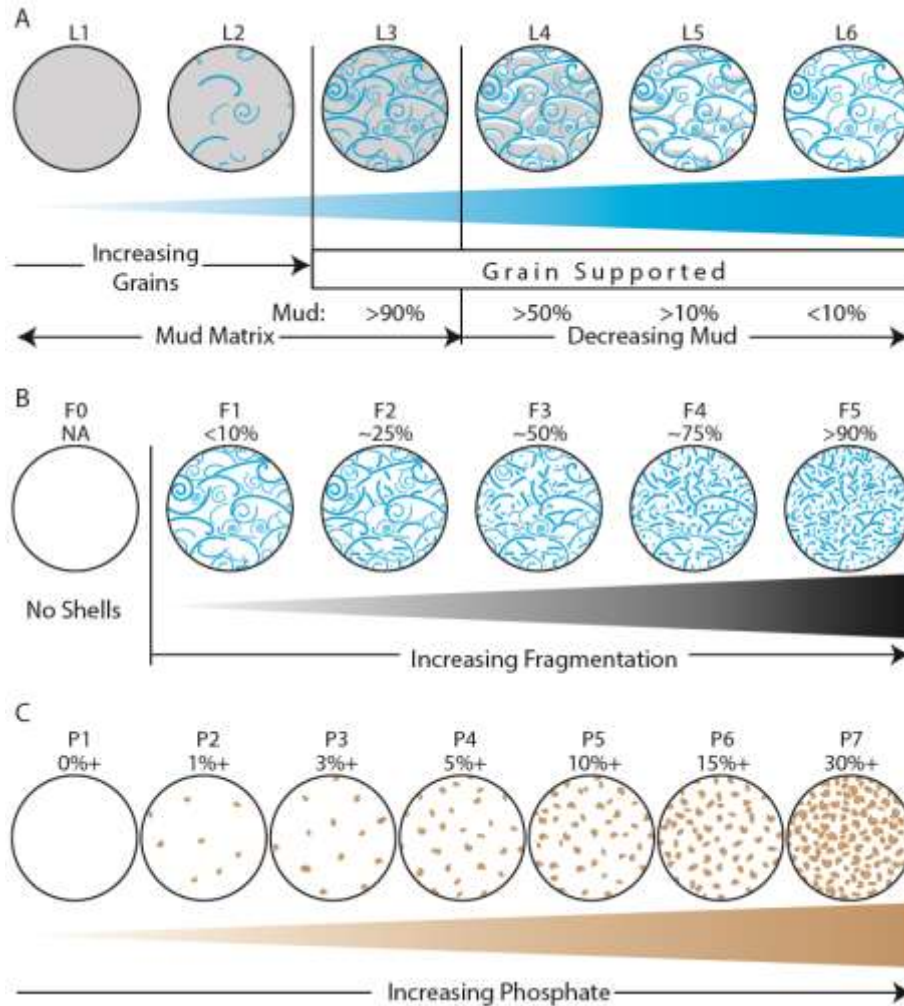
3.3.1. Carbonate classification

Figure 7.—Estimation standards. A. Lithological classification of coarse shell gravel. L1 micrite with no fossils, L2 mud supported rock with few fossils, L3 fossil supported with more than 90% mud in matrix, L4 fossil supported with more than 50% mud in matrix, L5 fossil supported with less than 50% mud in matrix, and L6 fossil supported with less than 10% mud in matrix. B. Visual estimation of fragmentation approximating the percentage of thin-section sample area occupied by fragments/total shell volume. F0 = no shells available for observation, F1 = less than 10% area fragmented, F2 = approximated 25% fragmented area, F3 = approximately half fragmented, F4 = approximately 75% fragmented, and F5 = greater than 90% fragmented. C. Visual estimation of percent volume phosphatic particles based on Shvetsov (1954) and Terry and Chilingar (1955). P1 = less than 1%, P2 = 1% to less than 3%, P3 = 3% to less than 5%, P4 = 5% to less than 10%, P5 = 10 % to less than 15%, P6 = 15% to less than 30%, and P7 = 30% or greater.

The vast majority of Cincinnatian carbonates of this study fall roughly into the same broadly

defined microfacies (e.g. Flügel, 2012) of reworked shell beds. As such, they are grain-supported

bioclastic, mostly shell-bryozoan rudstones (*sensu* Embry and Klovan, 1971). Peloids made of micrite are

present but rare, are sand sized, and tend to occur in sheltered areas within or beneath shells. Ooids and

lithoclasts, except for shale rip-up clasts, are absent in all but the most condensed lithologies (e.g. Fig. 4).

Bioclasts are mostly brachiopods, bryozoans, disarticulated echinoderm ossicles, gastropods (mostly

aragonitic) and bivalves (mostly aragonitic). Carbonate silt, consisting of bioclasts <0.062 mm, is

obviously an in-place product of fragmentation in most carbonates. Silt is also the coarsest transported

component, as evidenced by well-sorted, laminated calcisiltite beds.

Given this degree of uniformity of bioclasts, the greatest variability is in the degree to which mud

(micrite and calcisiltite) fills the intershell spaces. We established our own classification system to

distinguish a range of mud-dominated versus spar-dominated lithologies. Given the small variability in

microfacies, any further distinctions between lithologies would require at least gross taxonomic

quantification of the bioclasts, not undertaken in this study.

We devised a rudstone classification (shells >2mm = rudstone) because most of the rocks contain

significant proportions of large shells (Fig. 6A). We determined fabric as shell supported or not, and if

shell supported, classified further by the proportion of space between the shells that was filled with mud

(including calcisilt). The six resulting classes are L1) matrix = micrite and calcisiltite 100%, no shells,

L2) matrix supported, some shells, L3) shell supported, more than 90% lime mud in the matrix), L4) more

than half lime mud in the matrix, L5) less than half lime mud in the matrix, and L6) less than 10% lime

mud. One coauthor (MF) classified lithology for all thin-section samples for consistency.

3.3.2. Shell fragmentation

Shell fragmentation was visually estimated (Fig. 7), and classified into six shell fragmentation

classes: F0) no shells observed; no fragmentation observed. F1) all whole shells, F2) mostly (>75%)

whole shells, F3 about half fragmented, F4) mostly fragmented (>75%) and F5) nearly all fragmented.

Given that F0 (no shells) is not a measure of fragmentation, these were dropped from most statistical

analyses. Given that the thin-section samples were unevenly distributed among the original categories, we

combined categories to a minimum of 39 thin-section samples for statistical analyses. One coauthor (MF) classified all of the thin-section samples for consistency.

3.3.3. Phosphate grain recognition

Phosphatic microsteinkerns are composed of CFA that fills cavities, and generally range in size from 0.25 to 1.5 mm in diameter or minimum width. Preliminary work in recognizing these particles (Dattilo et al., 2015, 2016, 2018) utilized EDS scans of thin sections and dissolution with acetic acid to liberate non-soluble phosphatic residue. We determined that we could visually identify phosphatic steinkerns with confidence from thin sections in these rocks; no other materials have precisely the same optical properties and shapes/habits (Fig. 6C, D). Phosphatic skeletal elements such as lingulate brachiopods and conodonts can be distinguished by their lighter yellowish color, translucency, and laminations that arise from skeletal accretion as well as the consistently tabular outlines. Ferroan dolomite and ankerite resemble CFA but tend to be more diffuse in distribution and more transparent; they are not found specifically as steinkerns. Rounded, unidentifiable, but amorphous CFA particles were counted along with obvious steinkerns.

Molded echinoderms presented a particular challenge for counting. Definitive optical identification of stereomic molds is most easily accomplished by the use of ultrathin (10—15 micron) thin sections to clearly see the fillings of the 10-micron stereom fabric without obstruction by trabecules covering the filled area in the z axis. However, most sections are not this thin, so that instead it depends upon recognition of stereomic structure made visible by the optical contrast with dark phosphate. The more typical syntaxial calcite filling is optically identical to the stereom, so it obscures stereomic structure. This is a potential source of error, as lightly-colored stereomic molds of ossicles are difficult to distinguish from calcite filled stereom with only the typical inclusions in cement as contrast.

3.3.4. Grain estimation

Our emphasis is on number of microfossils and other CFA particles rather than volume of phosphate. Nevertheless, the consistent size of these sediment particles (0.25–1.5 mm) allows grain count to be taken as a proxy for volume and vice versa. We performed visual volume estimation to test whether or not this more rapid method is adequate as a substitute for counting. This procedure required training coauthor MF to estimate relative grain volumes visually by comparison to our standard charts (Fig. 7C; based on Terry and Chilager, 1955). This coauthor (MF) had experience with a related data set (from a significantly higher stratigraphic position) of 200+ thin-section samples (Frauhiger et al. 2018) and estimated volumes for every thin-section sample used in this dataset.

3.3.5. Grain counting

We counted grains within the 4 cm^2 area (e.g. Fig. 6C, 6D) selected for each thin-section sample using a petrographic polarizing microscope in tandem with the previously scanned image. This required an observer to both distinguish and count phosphatic microsteinkern grains. If recognized as phosphatic infilling, each individual grain was counted. If a large number of zooecia of a single bryozoan colony fragment in the thin-section sample was encountered, every filling was counted, a source of anomalously high counts, but single fragments of bryozoans dominated very few thin-section samples. In contrast to bryozoans, other phosphatic micromolds were more evenly dispersed within a given sedimentary unit.

The time required to learn and perform this work necessitated the use of four different researchers (coauthors AS, MF, AH, and LS) with some overlap. The resulting data file is available online (Supplemental File 1). When an observer questioned their identifications, BFD checked the work. Where overlap existed, we noted consistent but not perfectly identical counts, with some very high counts that were inconsistent with visual estimation. For the purposes of this study, we chose the lowest count for each thin-section sample that two or more researchers had counted. An analysis of potential sources of error related to differences in individual's counts is available online (Supplemental File 2).

One type of error that may have contributed to discrepancies occurred when non-phosphatic particles or areas were mistaken (because of similar color, for example) for phosphatic microsteinkerns and included in the final count, especially where counts were very high. Another error was failure to recognize and count phosphatic particles, which was particularly difficult with some of the lighter colored stereomic molds of echninoderm ossicles. Some thin-section samples contain no visually recorded phosphatic steinkerns, but a few of the same limestone blocks have yielded steinkerns from acid residues (depending on the amount of rock dissolved, this method "samples" far more of the rock than a 4 cm^2 thin-section sample can) from previous work (Dattilo et al., 2016). This discrepancy suggests that a few steinkerns per thin-section sample is a detection limit, and that results obtained through either visual estimation or counting that result in no microsteinkerns should be considered as "not detected" rather than "0". If larger areas of, for example, 8, or 16, or 32 cm^2 had been counted, then steinkerns may have been detected.

3.3.6. Statistical treatment

The resulting phosphatic grain counts and estimated phosphate percent volume classes were parsed into the lithologic and fragmentation classes in separate analysis with the goal of determining if there is a progressive relationship between ordinal phosphate classes and ordinal classes representing maturity by lithology or by fragmentation. Grain counts (quantitative) plotted against ordinal categories of fragmentation or lithology required one sort of analysis. Grain volume estimates (ordinal categories) plotted against the same ordinal categories of lithology and fragmentation required a different approach.

3.3.7. Testing grain volume estimates against proxies for maturity

We used contingency tables calculated in Microsoft Excel spreadsheets to plot grain volume estimates against fragmentation and lithology (two-way contingency tables), and to plot all grain volume, fragmentation, and lithology against each other simultaneously (three way contingency table). We used these plots to explore the question of whether there is a positive relationship between inferred maturity of

the sediment and percent volume of phosphatic microsteinkerns. Two Chi-squared tests might address such a problem. In the Chi-squared goodness of fit test, observed distribution in the contingency table is compared to a predetermined theoretical distribution. While our sedimentological model does predict that more phosphatic grains will be found in association with more mature lithologies or more fragmented shells, the precise distribution is not predicted so this test is not possible.

The Chi-squared test of independence can test the null hypothesis that the two sets of categories (phosphate vs. lithology or vs. fragmentation, or lithology vs. fragmentation) are completely independent, which is a distribution that can be calculated from any contingency table without an *a priori* model of distribution. If the rows and columns are independent, then the expected value of each cell is given by

$$exp = \frac{(row\ total) \times (column\ total)}{total\ sample\ size} \tag{1}$$

here and column and row totals are the total number of cells with the same variable 1 and variable 2 value respectively.

All three sets of categories (phosphate vs. lithology vs. fragmentation) can also be tested and the expected value of each cell is calculated the same method expressed here more generally

$$exp_{LFP} = \frac{(\sum_{f=0}^{5}\sum_{p=1}^{7} obs_{Lfp}) \times (\sum_{l=1}^{6}\sum_{p=1}^{7} obs_{lFp}) \times (\sum_{l=1}^{6}\sum_{f=0}^{5} obs_{lfP})}{N^2} \tag{2}$$

where *exp* = expected value, *obs* = observed value, and *exp* subscripts *L*, *F*, and *P* are the specific value of lithology, fragmentation, and phosphate respectively corresponding to *obs* indices *l*, *f*, and *p*, and N = total statistical sample size (total number of thin-section samples).

For the Chi-squared test of independence to be valid, the expected count for each cell in the contingency table should be greater than 5. Initial two-way runs using original data classes left many cells below predicted value of 5, and many below a predicted value of 1. This was a result of both the rarity of high volumes of steinkerns and the rarity of extreme lithologies (L1, L2, and L6), as well as very low fragmentation proportions (F1, F2) in the dataset.

To meet the assumption of expected counts greater than 5 and to maintain the ordinal character of the categories, adjacent lowest populated columns were combined pair-wise from the extreme ends of the ordinal spectrum for lithologies, and from the low end for fragmentation, and from the high end for phosphate. Then two-way contingency tables and predicted values of each resulting cell were recalculated. This was repeated until all predicted cell values exceeded 5, resulting in combined categories as discussed previously. Combining categories in the same way for the three-way contingency table still resulted in a large number of cells with predicted values below 5, making it impossible to rigorously test the significance of the three way table, though it still provides a valuable visualization.

Chi-squared statistics and p values were calculated for all two-way contingency tables after combining rows and columns. While this test can be used to demonstrate that two sets of categories are not assorted independently among the thin-section samples, it does not reveal the structure of the dependence, which is really the question of interest.

To obtain information on what the actual pattern of dependency is between phosphate content and the two proxies for shell bed maturity, we calculated the standardized residual (also called Z-score) for each cell in the full and the compressed contingency tables.

$$Z = \frac{(obs - exp)}{\sqrt{exp}} \tag{3}$$

Using the general guideline that the Z standardized residuals are treated as if they come from a standard normal distribution (bell-shaped with mean 0 and standard deviation 1; Agresti, 2002) with symmetry about zero, we shaded cells red for positive, blue for negative, and white for zero, with increasing color saturation with distance from zero, flagging cells with standardized residuals exceeding 2 in absolute value (approximating $p = 0.05$) with fully saturated colors.

Standardized residuals show which cells contain more or less thin-section samples than expected, but cannot indicate "correlation" between the different sets of categories. Spearman's rank (cor.test in R;

Spearman, 1904; Holander and Wolf, 1973) was used to measure the strength of the association in each of the contingency tables.

3.3.8. Testing grain counts against proxies for maturity

The distributions are non-Gaussian and for this reason nonparametric procedures were used. The Kruskal-Wallis test (Kruskal and Wallis, 1952; Hollander and Wolfe, 1973) in R (kruskal.test) was used to test the null hypothesis of equal medians across the fragmentation groups and the lithologies, separately. Dunn's multiple comparison procedure (Dunn, 1964) with p-values adjusted using the Benjamini-Hochberg method (Benjamini and Hochberg, 1995; dunn.test in R) was used to follow up on which specific pairs differ significantly. Ninety-five percent confidence intervals for the group medians were computed using a bootstrap routine in R based on 5000 bootstrap samplings of the data set.

4. Results

4.1. Estimated lithology, fragmentation, and phosphate vary together

We generated three series of visually estimated ordinal categorical data from the 267 thin-section samples: series 1 lithology (L, six ordinal categories), series 2 fragmentation (F, "0"-no shells, plus five ordinal categories), and series 3 phosphate content (P, seven ordinal categories). Detailed results of the analysis of ranked category data are available online (Supplemental File 3). For some analyses, because of the low number of observations in those categories, the lowest-occurring ordinal categories of each series were combined (preserving ordinal value) into three (L and F) or four (P) new composite categories (CL, CF, CP) each. We could test these composite categories without violating statistical assumptions: lithology, CL = L1+L2+L3, CL2 = L4, CL3 = L5+L6; fragmentation, (F0, no shells was dropped), CF1 = F1+F2+F3, CF2 = F4, CF3 = F5; phosphate; CP1 = P1, CP2 = P2, CP3 = P3+P4, CP4 = P5+P6+P7.

We compared these series pairwise in all possible combinations (P vs L, P vs F, and F vs L). All three pairs showed positive associations suggesting that thin-section samples falling into the lower ordinal

category of one series are likely to also fall into lower ordinal categories of the other two series, and likewise for the middle and upper categories. In other words, greater spar content (lack of mud) is associated with greater fragmentation and both are associated with higher phosphate content.

Statistically this relationship is supported by chi-squared tests, standardized residuals of observed versus predicted occurrences, and Spearman's rank correlation (Spearman, 1904). Chi-squared statistics suggest much greater than 99% confidence that the relationships between these series is not random. "Not random" does not specify a relationship, but the chi-squared test includes a predicted value for every possible combination of categories in pairwise comparisons, and these expected values provide a hint to actual relationships between the categories. The standardized residual (Z-score) is a measure of the degree to which the observed occurrences of a given combination of categories is greater or less than expected. Z-scores suggest that the number of thin-section samples observed to contain nearly corresponding L, F, and P values are higher than expected with 95% confidence, while the number of thin-section samples falling into different categories for L, F, and P (statistically valid for composite categories) were lower than expected at 95% confidence. The final support for this relationship comes from Spearman's rank correlation, which varies pairwise from 0.597 to 0.702, all moderately sized positive associations, and all supported at greater than 99% confidence ($p < 0.001$).

4.2. Phosphatic SSF grain counts also vary with lithologic maturity and fragmentation

Phosphatic grain count data confirms the relationships that estimated phosphate demonstrates. We analyzed count data by grouping thin-section samples into their composite lithology (CL) and fragmentation (CF) categories as described in Section 4.1. A detailed discussion of grain count analysis results is available online (Supplemental File 4). Thin-section samples that fall into higher ranking lithologies or fragmentation tend to have higher phosphate grain counts. In both cases, the histograms show non-normal, possibly polymodal distributions. One of the modes for each sub-distribution (by lithology or by fragmentation class) is "0" or "not detected". Each successive decrease in mud content and each successive increase in fragmentation is characterized by the rightmost mode moving farther to

the right (higher grain counts), as well as a decrease in the peak height of the "Not Detected" mode to the left.

We applied the Kruskal-Wallis test across the three composite categories of lithology and across the three categories of fragmentation. In each case, the test suggests that grain count medians differ with greater than 99% confidence ($p < 0.001$) Dunn's test applied to each pair of lithology-grouped and to each pair of fragmentation-grouped thin-section sample counts shows a significant difference for every pair at greater than 98% confidence. This result confirms that increasing spar content and increasing fragmentation are each associated with increasing numbers of phosphatic particles.

4.3 Visualizing shell bed maturity and phosphate content

The three-way contingency table (Fig. 8) shows the distribution of the thin-section samples in three-dimensional lithology (L)-fragmentation (F)-phosphate (P) space without combination of categories. This fully expanded three-way table has few cells with expected values >5, but standardized residuals (Z scores) in some cells are high enough that the three-dimensional representation provides a worth-while illustration of the overall distribution of thin-section samples along the diagonal. By lining up thin-section sample images (Fig. 9, thin-section samples numbered as in Fig. 8 cells) from low L, F, and P cells the progressive correspondence between lithology, fragmentation, and phosphate along the three-way table diagonal is clear.
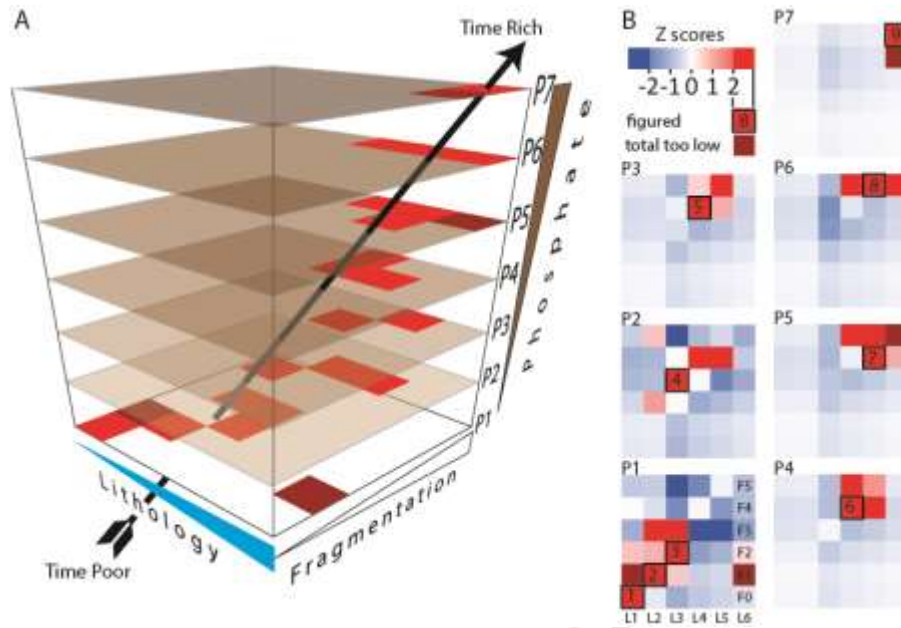
Figure 8—All observed thin-section samples represented as Z-score heat maps in the three dimensions of visually estimated lithology (L), fragmentation (F), and phosphate content (P). Each phosphate category (P1 through P7) is represented as a square grid of fragmentation (F0 – F5) versus lithology (L1 – L6). A) 3 dimensional plot with grids stacked vertically in perspective view with highest positive Z scores highlighted in red (predicted values ≥5) or pink (predicted values <5). Diagonal arrow indicates inferred "correlation" trend, and is interpreted as indicating time richness. B) Map view of the same seven grids, represented as Z-score heat maps with saturated blue representing scores < -2, saturated red representing score >2, and white representing scores = 0. High scores with predicted values < 5 are shaded. Outlined-and-numbered cells (1 – 9) represent progressive textural maturity, fragmentation, and phosphate . Numbered images of one thin-section sample from each of these cells shown as part of a thin-section sample progression (Fig. 9).
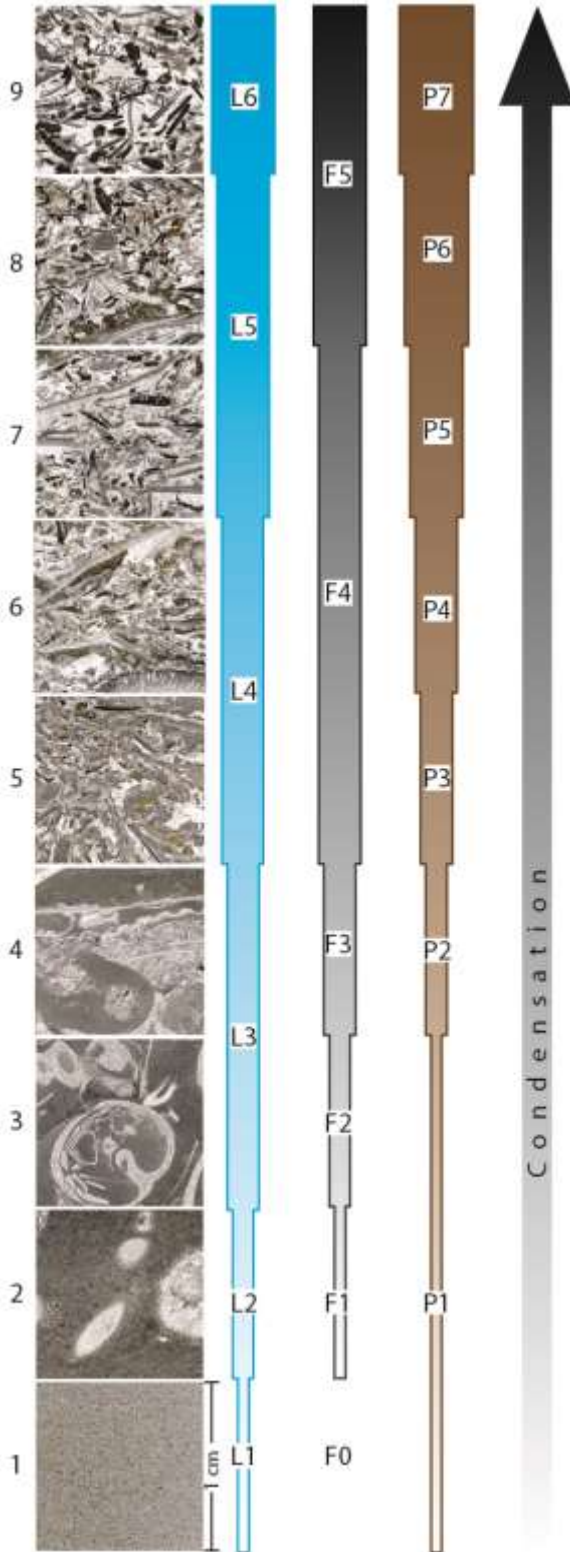
Figure 9.—Thin-section sample progression following the diagonal of the three-way contingency table (Figs. 8). Numerals in the left column correspond to the numbered cells (Fig. 8B). Each image is a scan of 1 cm^2 of one thin-section sample from the numbered cell, the blue stepped triangle represents increasing textural (lithology) maturity (L1 – L6), the black triangle represents increasing fragmentation (F0 – F5), and the brown represents increasing phosphate (P1 – P7). The black arrow on the right represents the interpreted direction of increasing condensation/time-richness that drives textural maturity, fragmentation, and phosphate accumulation.

5. Discussion

5.1. Phosphatic steinkerns are related to textural maturity

Our research demonstrates that phosphatic microsteinkern concentration, measured by both visual estimation and by grain counting, is strongly correlated with textural maturity, whether that maturity is measured by fragmentation or by lithology. The confidence intervals ($p < 0.001$) resulting from Chi-squared analysis suggest a very small probability that these co-occurrences resulted from the chance combination of independent factors.

Beyond simply demonstrating that microsteinkern concentration and maturity are correlated, we also show that their correlation is positive: an increase in textural maturity as measured by either fragmentation or lithology correlates with an increase in phosphate, as measured either by counts or by visual estimation. The significant separation of median phosphate grain count values for each of the fragmentation or lithology categories in succession demonstrates this relationship. The significantly higher-than-expected values in the up-trending diagonal cells plus the significantly lower-than-expected values of remaining cells in phosphate versus fragmentation or phosphate versus lithology contingency tables (Supplemental File 3), as confirmed by Spearman's rank test also support this interpretation. The hundred- to thousand- fold increase in phosphate grain concentration is more than can be expected from grain-packing effects of shell fragmentation, and can best be explained by the addition of phosphate grains, the destruction of carbonate grains, or both.

These results corroborate the hypothesis that a single mechanism either directly generated or coordinated the generation of textural maturity and phosphate in these shell bed limestones. We also conclude that this mechanism acted to increase microsteinkern concentration as it decreased mud content of the shell beds and increased fragmentation of the shells.

5.2. The PPC model explains both shell beds and phosphate accumulation

5.2.1. Time-richness is another mechanism for textural maturity

The application of the concept of "time-richness" (Brett and Baird, 1993) to Cincinnatian shell beds arose from a revised view of process sedimentology of Cincinnatian shell beds and meter-scale cycles of carbonate-rich and mudstone/shale-rich phases. This revised model is called "episodic starvation shell bed (ESSB) model" and attributes shell bed accumulations to periods of low siliciclastic influx during which shell accumulations accrued on the seafloor and were occasionally disturbed by high-energy, storm-related events. Phosphatic microsteinkerns were reported and considered as diagenetic evidence for more extreme bed-scale condensation (Brett et al., 2008; Dattilo et al., 2008).

The tempestite proximality model (Aigner 1982, 1985) for shell bed accumulation implies a direct correspondence between depositional environment (depth and energy) and textural maturity. Assuming that such a direct depth-maturity relationship is correct, this mechanism would still not provide enough time to repeatedly (every new shell bed) generate new phosphatic grains and then rework them. Even assuming that certain geochemical fluctuations led to very rapid precipitation of phosphatic particles, the connection between the geochemical process and the high-energy environments is missing.

Long range transport could explain textural maturity but this mechanism was also rejected for the Kope Formation (Brett et al., 2008), and the current study interval (Dattilo et al., 2008). Evidence for lack of transport includes the correlation of single beds for hundreds of kilometers parallel to depositional strike, which poses a serious source and mass balance problem for any interpretation of transport. Further evidence includes the very poor sorting of the shell beds and the preservation of small-scale fossil patchiness (Miller, 1997). Those deposits that do include evidence of transport tend to be no coarser than silt size, including well sorted laminated calcisiltites, siltstones, and mudstones, but not coarser carbonates. Long range transportation could conceivably result in a correlation between shell bed maturity and phosphatic steinkern content, provided that there is a source of steinkerns to concentrate (e.g. Föllmi, 1990). However, no such source of steinkerns has been located. Furthermore, phosphatic material is typically more concentrated in low energy, offshore facies where offshore transport would be anticipated to be least effective.

5.2.2. Time-richness and phosphatic sediments

The serendipitous discovery of very low concentrations of microsteinkerns during a shell bed taphonomic study (Freeman et al., 2013) led to the hypothesis that phosphogenesis was a slow geochemical process operating under normal marine conditions (Dattilo et al., 2016). The PPC process (Freeman et al., this volume) explains how this slow process leads to the accumulation of phosphatic microsteinkerns as the shell bed develops, through iterative precipitation and reworking events, resulting in strong correlations between textural maturity and phosphatic microsteinkern concentration. Time-richness (stratigraphic condensation) is the unifying concept that explains both textural maturity and steinkern accumulation under this model.

The PPC model is partly based on the idea of Baturin cycles (Baturin, 1971; Mullins and Rasch, 1985; Föllmi, 1996; but see Pufahl et al., 2003). These cycles are tied to sea-level changes and require two separate phases—one a quiet, deeper-water phase for phosphate development in the sediment, and the other a high-energy phase for phosphate concentration through the winnowing of finer sediment during times of lower sea level. Application of the Baturin cycles to Cincinnatian shell beds without alteration would imply that muddy lithologies as representing unwinnowed phases where some steinkerns grew but were not concentrated, while the sparry lithologies would represent the second phase of concentration of steinkerns facilitated by shallow-water winnowing. But again, this mechanism would require rapid and major changes in sea level.

The ESSB model allows the application of a cyclic process without invoking major shifts in sea level to generate each bed. The PPC model can be visualized as a two-phase process that episodically repeats itself. It provides a more parsimonious explanation for the coordination of textural maturity and phosphate concentration. True Baturin cycles would require longer periods of quiet phase phosphogenesis to be followed by shallowing and more intense reworking. The PPC process requires longer periods of low sedimentation, or a shallowing event, either of which will result in a higher incidence of phosphogenesis-event reworking cycles.

Witzke (1987) and Witzke and Heathcote (1997) proposed that phosphogenesis in the Upper Ordovician Elgin Limestone of Iowa resulted from precipitation at the interface between deeper oceanic dysoxic waters and the shallower oxic waters of the epeiric sea. One important component of this interpretation was the apparently dwarfed fauna found in this midcontinental strata as evidenced by abundant phosphatic micro-steinkerns (Witzke and Heathcote, 1997). Dattilo et al (2016) argued that the small size of similarly preserved Cincinnatian fossils is the result of taphonomic bias, not a specialized diminutive fauna. Reeder et al. (2015) also examined the phosphatic fossil fauna of the Elgin Limestone of Iowa and found the same taphonomic bias. This model could explain the coordination of phosphate content and textural maturity if mixing occurred near the seafloor above fair-weather wave base, but the fact that Cincinnatian grainstones tend to be more abundant in deeper-water deposits also speaks against this process.

Given plausible time scales for deposition of shell bed limestone units, ranging from 10^2 to 10^4 years (Brett and Algeo, 2001), changes in water mass chemistry could certainly have occurred. Some water mass conditions could be more favorable to the formation of phosphatic particles than others, but a scenario in which every single phosphate-bearing shell bed meshes perfectly with a specific fluctuation in water mass chemistry is implausible. The chemistry of an oceanic water mass is not linked to localized energy conditions on the seafloor.

5.2.3. Phosphate accumulation is evidence of time-richness

The above discussion of the process model should not overshadow the conclusion that lithofacies reflect the degree of condensation (i.e. time-richness) as much as, or more than, they reflect fair-weather energy conditions (Figs. 8, 9). The conclusion that carbonate textural maturity in the Cincinnatian is a measure of time-richness (Dattilo et al. 2008; Brett et al. 2008) is strongly supported by the correspondence between textural maturity and phosphatic steinkern concentration. The slow pace of phosphate enrichment of sediments is well documented (e.g. Föllmi, 1996). This observation is profoundly significant in its broad implications for the interpretation of carbonate microfacies beyond the

Cincinnatian. In contrast to siliciclastic sediments, carbonate sediments faithfully record time-richness because they generally originate in the basin of their deposition, and their individual grains are almost always geologically "new". While diagenetic minerals can inform the time-richness of a siliciclastic deposit as well (e.g. Glenn and Arthur, 1990; Baird and Brett, 2002), the siliciclastic sediments themselves cannot be used to detect time-richness. Siliciclastics are better sorted because they are transported into the basin hydraulically which prevents larger grains from reaching the offshore marine environment of deposition (e.g. Hjulstrom, 1935; Komar, 1989; Carling et al., 1992). Siliciclastics cannot be reliably used to gage the effects of grain aging in place (fragmentation, abrasion) because they come into the basin as already ancient particles, bearing the marks of weathering, erosion, and transport, perhaps through multiple cycles (e.g. Blatt, 1967; Blatt and Jones, 1975). The present study demonstrates that caution should be exercised when making direct comparisons between processes that operate in siliciclastic systems and those that are influential in carbonate sediments.

5.2.4. Time-richness: necessary, but not sufficient?

In application of the current findings to phosphatic sediment-yielding strata beyond the Cincinnatian, an important consideration is that time-richness alone does not assure phosphogenesis. There are many condensed deposits, especially in pure carbonate sediments, in which phosphatic grains are rare or absent. Other factors, well understood or postulated, are necessary for CFA to precipitate (e.g. Föllmi, 1996; Delaney, 1998; Paytan and McLaughlin, 2007; Filipelli, 2008). Texturally mature limestones that are apparently devoid of phosphatic sediments altogether exist even within Cincinnatian strata.

Several factors may have contributed to Cincinnatian phosphogenesis. The abundance of iron-rich clay (Scotford, 1965) is critical, because phosphogenesis requires iron; phosphorous is alternately concentrated on iron oxyhydroxides by adsorption under oxic conditions and released as conditions become more dysoxic (reducing), the so-called "iron pumping mechanism" (Berner, 1973; Shaffer, 1986; Froelich et al., 1988; Ingall and Jahnke, 1997; Heggie et al., 1990; O'Brien et al., 1990; Feely et al., 1991,

1998; Delaney, 1998; Poulton and Canfield, 2006). Thus, ironically, despite the dependence of phosphate concentration upon siliciclastic starvation, the presence of some terrigenous sediments may be a prerequisite to phosphate precipitation. Consequently, we postulate that phosphatic steinkerns may be largely absent in pure limestones, but strongly favored by mixed siliciclastic-carbonate facies.

Additionally, without an oxic/dysoxic boundary (in the sediments, in the case of the PPC process), this "iron pumping mechanism" does not function. Cincinnatian seas certainly had the necessary mix of aeration and biotic oxygen demand (in the sediment at least) to create appropriate redox gradients. Finally, the Cincinnatian is well-known for its rich marine invertebrate fossils (e.g. Cummings, 1908; Caster et al., 1955; Pojeta et al., 1979), evidence of abundant bioproduction, which requires nutrients (including phosphorus), and without which, sufficient phosphorus to produce significant phosphogenesis is unlikely to reach the sediment (e.g. Filipelli, 2008).

Even within the Cincinnatian strata—and in this data set—some thin-section samples do not conform to the pattern of strong correspondence between textural maturity and microsteinkern concentration. Thin-section samples with similarly high textural maturity contain a wide range of microsteinkern densities even as counted by the same person; a few are devoid of phosphatic microsteinkerns altogether. Some of this spread may be attributable to the fact that some periods between high-energy reworking and reburial events did not result in phosphogenesis, despite the high-energy events and intervening biotic activity contributing to winnowing and shell breakage. These non-phosphogenic periods may be related to a lack of critical factors cited above (iron from siliciclastic sediments, oxic/dysoxic gradients, burial of organic materials) or might be attributable to other geochemical or environmental parameters (e.g. Föllmi, 1996; Delaney, 1998; Paytan and McLaughlin, 2007; Filipelli, 2008). In the case of the Katian strata in the Cincinnati region, the local influx of elemental nutrients from the nearby Taconic Orogen is sufficient.

To summarize, many factors must coordinate to generate phosphatic grains. Any one of these factors is necessary, but not sufficient. The lack of phosphatic grains in texturally mature limestones does

not falsify the hypothesis that textural maturity in that depositional system is a product of sedimentary condensation.

5.3. Local conditions explain phosphatic SSFs in the Cincinnati Ordovician.

The PPC model (Freeman et al., this issue) is the geochemical consequence of the episodic starvation shell bed model (Dattilo et al., 2008; Brett et al. 2008). The PPC model for the generation and concentration of phosphatic microsteinkerns is based in part on the widely cited Baturin model for phosphatic sediment formation and concentration (Baturin 1971), but differs in that the two steps in the Baturin model (phosphogenesis and phosphate deposition), are envisioned by the PPC model as recurring processes that occur during sedimentary condensation within environments, not necessarily tied to changes in sea level. These processes result from event burial that triggers phosphogenesis, followed by subsequent event reworking that results in phosphate concentration, then reburial that begins the next round. The length of time that the shell bed develops on the seafloor before final burial by a major influx of siliciclastic sediments determines the number of reworking events to which the shell bed is exposed, with more events leading to both increased textural maturity of the resulting carbonate sediments and an increasing concentration of phosphatic microsteinkerns.

This conclusion is compatible with the observation that SSFs are generally associated with signs of reworking and condensation (Freeman et al., this volume) and lends support to the hypothesis that such an iterative process model can be applied more broadly, avoiding the need to invoke two separate and functionally independent phases of deposition to explain all occurrences.

The fact that abundant phosphatic sediments—mostly steinkerns—are strongly correlated with textural maturity also supports the conclusion that carbonate textural maturity may result from prolonged exposure at the seafloor mediated by episodic reworking by storms as much as, or more than, from the fair-weather energy of the depositional environment, as typically interpreted. This correlation is possible because the formation and accumulation of phosphate-rich sediments is a slow process.

Sedimentary condensation may generate textural maturity in carbonates without generating phosphatic sediments. Nevertheless, shell sands in these settings may owe their textural qualities more to long term exposure to multiple high energy reworking and burial events in an otherwise calm environment than to constant high energy conditions, generating heavily reworked shell bed grainstones that lack phosphatic sediments.

Highly reworked shell beds—rich in phosphate, or not—are the predictable outcomes of long intervals of accumulation and reworking of shells on the seafloor during periods of low sediment input, a prediction of the episodic starvation shell bed model.

The PPC model suggests that phosphatized small shelly fossils can form under normal marine conditions. Redox gradients can form by burial and decay of organic material in otherwise oxidized sediments. The necessary iron can be supplied from sediment derived from nearby terrigenous sources. Thus, the abundant phosphate of the midcontinent Ordovician is not necessarily the result of global marine dysoxia, or of increased iron content of the ocean, but reflects normal sedimentary processes and proximity to the Taconic highlands. Likewise, the globally high phosphate in the Katian may not reflect oceanic water mass changes so much as the accumulated local phosphate concentrations by normal sedimentological processes in the presence of iron supplied by a local uplift, one among globally numerous uplifts and volcanic terrains.

6. Conclusions

The polycyclic phosphogenic condensation (PPC) process emphasizes the role of residence time of sediments in the taphonomically active zone as a key factor in predicting the genesis and concentration of phosphatic microsteinkerns, a factor that should simultaneously influence carbonate textural maturity. We tested the hypothesis that these two seemingly unrelated phenomena would correlate with each other in Upper Ordovician strata of the Cincinnati, Ohio area by both estimating and counting phosphate grain concentration in over 250 thin-sectioned samples, as well as by examining two proxies of sediment

maturity: a) the degree of shell fragmentation, and b) lithological characteristics in terms of matrix/spar content of each thin-section sample, using an ordinal classification scheme. We found a strong positive relationship between phosphatic microsteinkern concentration and both measures of maturity. These correlations corroborate the hypothesis that phosphatic concentration is related to time-richness. Extremely low Chi-squared and Kruskal-Wallis p-values suggest a very small probability that this sample distribution was derived from a population in which fragmentation or amount of spar cement in carbonates is unrelated to phosphatic content. The PPC model is a more parsimonious explanation for the correspondence between textural maturity and phosphate content in these rocks than competing models that explain phosphogenesis and phosphorite concentration as separate events. Thus, the accumulation of phosphatic sediments is not necessarily a sign of unusual oceanic conditions, but can occur in normal ocean water as long as there is a supply of iron and other nutrients in the basin.

7. Acknowledgments

8. Data Availability

Data are available in four supplemental files.

9. References

Agresti, A., 2002. Categorical Data Analysis, Second Edition. Wiley, Hoboken New Jersey, pp. 78—83.

Aigner, T., 1982. Calcareous tempestites: storm-dominated stratification in Upper Muschelkalk

Limestones (Middle Trias, SW-Germany). In: Einsele, G., Seilacher, A. (Eds.), Cyclic and Event

Stratification. Springer, Berlin, pp. 180–198.

Aigner, T., 1985. Storm Depositional Systems: Dynamic Stratigraphy in Modern and Ancient Shallow

Marine Sequences. Lecture Notes in the Earth Sciences 3. Springer-Verlag, Berlin.

Aller, R.C., 1982. The effects of macrobenthos on chemical properties of marine sediment and overlying

water. In: McCall, P.L., Tevesz, M.J.S, (Eds.), Animal-Sediment Relations: The Biogenic

Alteration of Sediments. New York, Plenum Press, pp. 53–102.

Baird, G.C., Brett, C.E., 2002. Indian Castle Shale: late siliciclastic succession in the evolving Middle to

Late Ordovician foreland basin, eastern New York State. Physics and Chemistry of the Earth 27,

203–230. DOI: 10.1016/S1474-7065(01)00008-0

Baturin, G.N., 1971. Stages of phosphorite formation on the sea floor. Nature 232, 61–62. Doi:

10.1038/physci232061a0

Benjamini, Y., Hochberg, Y., 1995. Controlling the false discovery rate: a practical and powerful

approach to multiple testing. Journal of the Royal Statistical Society, Series B 57, 289–300.

Berner, R.A., 1973. Phosphate removal from sea water by adsorption on volcanogenic ferric oxides. Earth

and Planetary Science Letters 18, 77–86. Doi: 10.1016/0012-821X(73)90037-X

Blatt, H., 1967. Provenance determination and recycling of sediments. Journal of Sedimentary Petrology

37, 1031–1044. DOI: 10.1306/74D71825-2B21-11D7-8648000102C1865D

Blatt, H., Jones, R.L., 1975. Proportion of exposed igneous, metamorphic, and sedimentary rocks.

Geological Society of America Bulletin 86, 1085–1088. DOI: 10.1130/0016-

7606(1975)86%3C1085:POEIMA%3E2.0.CO;2

Brett, C.E., Algeo, T.J., 2001. Event beds and small-scale cycles in Edenian and lower Maysvillian strata

(Upper Ordovician) of northern Kentucky; identification, origin, and temporal constraints. In:

Algeo, T.J., Brett, C.E. (Eds.), Sequence, Cycle, and Event Stratigraphy of the Upper Ordovician and Silurian Strata of the Cincinnati Arch Region: 1999 Field Conference of the Great Lakes Section of the Society for Sedimentary Geology, Cincinnati, Ohio, Field Trip Guidebook 1, Series X11, 47–94.

Brett, C.E., Algeo, T., McLaughlin, 2003.The use of event beds and sedimentary cycles in high-resolution stratigraphic correlation of lithologically Repetitive Successions: The Upper Ordovician Kope Formation of Northern Kentucky and Southern Ohio: In P. Harries and D. Geary (eds.) High-Resolution Stratigraphic Approaches to Paleobiology, Kluwer Academic/Plenum Press.

Brett, C.E., Aucoin, C.D., Dattilo, B.F., Freeman, R.L., Hartshorn, K.R., McLaughlin, P.I., and Schwalbach, C.E., this volume. Revised sequence stratigraphy of the upper Katian Stage (Cincinnatian) strata in the Cincinnati Arch reference area: Geological and Paleontological Implications. Palaeogeography, Palaeoclimatology, Palaeoecology.

Brett, C.E., Baird, G.C., 1986. Comparative taphonomy: a key to paleoenvironmental interpretation based on fossil preservation. PALAIOS 1, 207–227. Doi: 10.2307/3514686

Brett, C.E., Baird, G.C., 1993. Taphonomic approaches to temporal resolution in stratigraphy: examples from Paleozoic marine mudrocks. In: Kidwell, S,M., Behrensmeyer, A.K. (Eds.), Taphonomic Approach to Time Resolution in Fossil Assemblages. Short Course in Paleontology 6, 250–274.

Brett, C.E., Hartshorn, K.R., Waid, C.B.T., McLaughlin, P.I., Bulinski, K.V., Thomka, J.R., Paton, T.R., Freeman, R.L., Dattilo, B.F., 2018. Lower to middle Paleozoic sequence stratigraphy and paleontology in the greater Louisville, Kentucky area. In: Flora, L.J. (Ed.), Ancient Oceans, Orogenic Uplifts, and Glacial Ice: Geologic Crossroads in America's Heartland. Geological Society of America Field Guide 51, 1–59.

Brett, C.E., Kirchner, B.T., Tsujita, C.J., Dattilo, B.F., 2008. Depositional dynamics recorded in mixed silicilastic-carbonate marine successions: insights from the Upper Ordovician Kope Formation of

Ohio and Kentucky, U.S.A. In: Pratt, B.R., Holmden, C. (Eds.), Dynamics of Epeiric Seas. Geological Society of Canada Special Paper 48, 73–102.

Brett, C.E., Malgieri, T.J., Thomka, J.R., Aucoin, C.D., Dattilo. B.F., and Schwalbach, C.E., 2015. Calibrating water depths of Ordovician communities: lithological and ecological controls on depositional gradients in the Upper Ordovician strata of southern Ohio and north-central Kentucky, USA. Estonian Journal of Earth Sciences 63, 1–15.

Brett, C.E., Seilacher, A. 1991. Fossil Lagerstätten: a taphonomic consequence of event sedimentation. In Einsele, G., Ricken, W., and Seilacher, A., eds., Cycles and Events in Stratigraphy. Springer-Verlag, Berlin, 284—297.

Carling, P.A., Kelsey, A. Glaister, M.S., 1992. Effect of bed roughness, particle shape, and orientation on initial motion criteria. In: Thorne, C.R., Bathurst, J.C., Hey, R.D. (Eds.), Sediment Transport in Gravel-bed Rivers, Wiley, Chichester, 23–37.

Caster, K.E., Dalvé, E.A., Pope, J.K., 1955. An Elementary Guide to the Fossils and Strata in the Vicinity of Cincinnati, Ohio. Cincinnati Museum of Natural History. 47 p.

Catuneanu, O., 2002. Sequence stratigraphy of clastic systems: concepts, merits, and pitfalls. African Journal of Earth Sciences 35, 1–43. Doi: 10.1016/S0899-5362(02)00004-0

Cook, P. J., McElhinny, M.W., 1979. A reevaluation of the spatial and temporal deposition of sedimentary deposits in light of plate tectonics. Economic Geology 74, 315–330.

Creveling, J.R., Knoll, A.H., Johnston, D.T., 2014a. Taphonomy of Cambrian phosphatic small shelly fossils. PALAIOS 29, 295–308. Doi: 10.2110/palo.2014.002

Creveling, J.R., Johnston, D.T., Poulton, S.W., Kotrc, B., März, C., Schrag, D.P., Knoll, A.H., 2014b. Phosphorus sources for phosphatic Cambrian carbonates. GSA Bulletin 126, 145–163. Doi: 10.1130/B30819.1

Cummings, E.R., 1908. The Stratigraphy and Paleontology of the Cincinnati Series of Indiana.Indiana Department of Geology and Natural Resources, 32nd Annual Report for 1907, 605–1189.

Dattilo, B.F., 1996. A quantitative paleoecological approach to high-resolution cyclic and event stratigraphy: the Upper Ordovician Miamitown Shale in the type Cincinnatian. Lethaia 9, 21–36. Doi: 10.1111/j.1502-3931.1996.tb01833.x

Dattilo, B.F., Brett, C.E., Schramm, T.J., 2012. Tempestites in a teapot? Condensation-generated shell beds in the Upper Ordovician, Cincinnati Arch, USA. Palaeogeography, Palaeoclimatology, Palaeoecology 367–368, 44–62. Doi: 10.1016/j.palaeo.2012.04.012

Dattilo, B.F., Brett, C.E., Tsujita, C.J., Fairhurst, R., 2008. Sediment supply versus storm winnowing in the development of muddy and shelly interbeds from the Upper Ordovician of the Cincinnati region, USA. Canadian Journal of Earth Sciences 45, 243–265. doi: 10.1139/E07-060

Dattilo, B.F., Freeman, R.L., Peters, W.P., Heimbrock, W.P., Deline, B., Martin, A.M., Kallmeyer, J.W., Reeder, J., Argast, A., 2016. Giants among micromorphs: were Cincinnatian (Ordovician, Katian) small shelly phosphatic faunas dwarfed? PALAIOS 31, 55–70. Doi: 10.2110/palo.2015.040

Davies, D.J., Powell, E.N., Stanton, R.J., Jr., 1989. Relative rate of shell dissolution and net sediment accumulation—a commentary: can shell beds form by the gradual accumulation of biogenic debris on the sea floor? Lethaia 22, 207–212. Doi: 10.1111/j.1502-3931.1989.tb01683.x

Delaney, M.L., 1998. Phosphorus accumulation in marine sediments and the oceanic phosphorus cycle. Global Biogeochemical Cycles 12, 563–572. DOI: 10.1029/98GB02263

Donoghue, P.C.J., Kouchinsky, A., Waloszek, D., Bengtson, S., Dong, X., Val'kov, A.K., Cunningham, J.A., Repetski, J.E., 2006. Fossilized embryos are widespread but the record is temporally and taxonomically biased. Evolution and Development 8, 232–238. Doi: 10.1111/j.1525-142X.2006.00093.x

Dornbos, S.Q., 2011. Phosphatization through the Phanerozoic. Taphonomy. Springer, Dordrecht, pp. 435–456.

Dunham, R.J., 1962. Classification of carbonate rocks according to depositional textures. AAPG Memoir 1, 108–121.

Dunn, O.J., 1964. Multiple comparisons using rank sums. Technometrics 6, 3, 241—252.

Dzik, J., 1994b. Evolution of 'small shelly fossils' of the Early Paleozoic. Acta Palaeontologica Polonica 39, 247–313.

Embry, A.F., III, Klovan, J.E., 1971. A Late Devonian reef tract on northeastern Banks Island, N. W. T. Bulletin of Canadian Petroleum Geology 19, 730–781.

Ettensohn, F.R., Hohman, J.C., Kulp, M.A., Rast, N., 2002. Evidence and implications of possible far-field responses to Taconian Orogeny: Middle to Late Ordovician Lexington Platform and Sebree Trough, east-central United States. Southeastern Geology 41, 1–36.

Feely, R.A., Trefry, J.H., Massoth, G.J., Metz, S., 1991. A comparison of the scavenging of phosphorus and arsenic from seawater by hydrothermal iron oxyhydroxides in the Atlantic and Pacific Oceans. Deep-Sea Research 38, 617–623. Doi: 10.1016/0198-0149(91)90001-V.

Feely, R.A., Trefry, J.H., Lebon, G.T., German, C.R., 1998. The relationship between P/Fe and V/Fe ratios in hydrothermal precipitates and dissolved phosphate in seawater. Geophysical Research Letters 25, 2253–2256. Doi: 10.1029/98GL01546.

Filipelli, G.M., 2008. The global phosphorus cycle: past, present, and future. Elements 4, 89–95. Doi: 10.2113/GSELEMENTS.4.2.89

Flügel, E., 2004. Microfacies analysis of carbonate rocks: Analysis, Interpretation and Application. Springer-Verlag Berlin Heidelberg. 976 pp.

Folk, R.F., 1959. Practical petrographic classification of limestones. Bulletin of the American Association of Petroleum Geologists 43, 1–38.

Föllmi, K.B., 1990. Condensation and phosphogenesis: examples of the Helvetic mid-Cretaceous (northern Tethyan margin). In: Notholt, A.J.G., Jarvis, I. (Eds.), Phosphorite Research and Development. Geological Society Special Publication 52, 237–252.

Föllmi, K.B., 1996. The phosphorus cycle, phosphogenesis and marine phosphate-rich deposits. Earth-Science Reviews 40, 55–124. Doi: 10.1016/0012-8252(95)00049-6

Freeman, R.L., Dattilo, B.F., Brett, C.E., this volume. An integrated stratinomic model for the genesis and concentration of "small shelly fossil"-style phosphatic microsteinkerns in not-so-exceptional conditions. Palaeogeography, Palaeoclimatology, Palaeoecology.

Freeman, R.L., Dattilo, B.F., Morse, A., Balir, M., Felton, S., and Pojeta, J., Jr., 2013. The "Curse of *Rafinesquina*": negative taphonomic feedback exerted by strophomenid shells on storm-buried lingulids in the Cincinnatian Series (Katian, Ordovician) of Ohio. PALAIOS 28, 359–372.

Froelich, P.N., 1988. Kinetic control of dissolved phosphate in natural rivers and estuaries: a primer on the phosphate buffer system. Limnology and Oceanography 37, 6, 1129–1145. Doi: 10.4319/lo.1988.33.4part2.0649

Froelich, P.N., Arthur, M.A., Burnett, W.C., Deakin, M., Hensley, V., Jahnke, R., Kaul, L., Kim, K.-H., Roe, K., Soutar, A., Vathakanon, C., 1988. Early diagenesis of organic matter in Peru continental margin sediments: phosphorite precipitation. Marine Geology 80, 309–343. Doi: 10.1016/0025-3227(88)90095-3

Glenn, C.R., Arthur, M.A., 1990. Anatomy and origin of a Cretaceous phosphorite-greensand giant, Egypt. Sedimentology 37, 123–154. DOI: 10.1111/j.1365-3091.1990.tb01986.x

Grabau, A.W., 1094. On the classification of sedimentary rocks. American Geologist 33, 228–247.

Heggie, D.T., Skyring, G.W., O'Brien, G.W., Reimers, C., Herczeg, A., Moriarty, D.J.W., Burnett, W.C., Milnes, A.R., 1990. Organic carbon cycling and modern phosphorite formation on the East Australian contiententental margin: An overview. In: Notholt, A.J.G., Jarvis, I. (Eds.), Phosphorite Research and Development. Geological Society Special Publication 52, 87–117. Doi: 10.1144/GSL.SP.1990.052.01.07

Hjulstrom, F., 1935. Studies in the morphological activity of rivers as illustrated by the River Fyris. Geological Institute Upsala 25, 221–528.

Holland, S.M., 1993. Sequence stratigraphy of a carbonate-clastic ramp: the Cincinnatian Series (Upper Ordovician) in its type area. Geological Society of America Bulletin 105, 306–322. Doi: 10.1130/0016-7606(1993)105%3C0306:SSOACC%3E2.3.CO;2

Holland, S.M., 1998. Sequence stratigraphy of the Cincinnatian Series (Upper Ordovician, Cincinnati. Ohio region). In: Davis, R.A., Cuffey, R.J. (Eds.) Sampling the Layer Cake That Isn't: Stratigraphy and Paleontology of the Type Cincinnatian. Ohio Division of Geological Survey, Columbus, Ohio, pp. 135–151.

Holland, S.M., 2008a. Climate-driven storm cyclicity: a non-eustatic mechanism for generating offshore meter-scale cycles. In: McLaughlin, P.I., Brett, C.E., Holland, S.M., Storrs, G. (Eds.), Stratigraphic Renaissance in the Cincinnati Arch: Implications for Upper Ordovician Paleontology and Paleoecology. Cincinnati Museum Center Special Publication 2, 166–172.

Holland, S.M., 2008b. The type Cincinnatian: an overview. In: McLaughlin, P.I., Brett, C.E., Holland, S.M., Storrs, G. (Eds.), Stratigraphic Renaissance in the Cincinnati Arch: Implications for Upper Ordovician Paleontology and Paleoecology. Cincinnati Museum Center Special Publication 2, 44–61.

Holland, S.M., Miller, A.I., Meyer, D.L., Datttilo, B.F., 2001. The detection and importance of subtle biofacies within a single lithofacies: the Upper Ordovician Kope Formation of the Cincinnati,

Ohio Region. PALAIOS 16, 205–217. Doi: 10.1669/0883-1351(2001)016<0205:TDAIOS>2.0.CO;2

Holland, S.M., Miller, A.I., Dattilo, B.F., Meyer, D.L., Dieckmeyer, S.L., 1997. Cycle anatomy and variability in the storm-dominated type Cincinnatian (Upper Ordovician): coming to grips with cycle delineation and genesis. The Journal of Geology 105, 135–152. Doi: 10.1086/515904

Holland, S.M., Patzkowsky, M.E., 1996. Sequence stratigraphy and long-term lithologic change in the Middle and Upper Ordovician of the eastern United States. In: Witzke, B.J., Ludvigsen, G.A., Day, J. (Eds.), Paleozoic Sequence Stratigraphy: Views from the North American craton. Geological Society of America Special Paper 306, 117–129. Doi: 10.1130/0-0837-2306-X.117

Holland, S.M., Patzkowsky, M.E., 2007. Gradient ecology of a biotic invasion: biofacies of the type Cincinnatian Series (Upper Ordovician) Cincinnati, Ohio region, USA. PALAIOS 22, 392–407. Doi: 10.2110/palo.2006.p06-066r

Hollander, M., and Wolfe, D.A., 1973. Nonparametric statistical methods. Wiley, New York, 848 p. Doi: 10.1002/bimj.19750170808

Ingall, E., Jahnke, R., 1997. Influence of water-column anoxia on the elemental fractionation of carbon and phosphorus during sediment diagenesis. Marine Geology 139, 219–229. Doi: 10.1016/S0025-3227(96)00112-0

Jahnke, R.A., Emerson, S.R., Roe, K.K., Burnett, W.C., 1983. The present day formation of apatite in Mexican continental margin sediments. Geochimica and Cosmochimica Acta 47, 259–266.

Jarvis, I., Burnett, W.C., Nathan, Y., Almbaydin, F.S.M., Castro, L.N., Flicoteaux, R., Hilmy, M.E., Husain, V., Quatawnah, A.A., Serjani, A., Zanin, Y.N., 1994. Phosphorite geochemistry: state-of-the-art and environmental concerns. Eclogae Geologicae Helveticae 87, 643–700.

Jennette, D.C., Pryor, W.A., 1993. Cyclic alternation of proximal and distal storm facies: Kope and
Fairview Formations (Upper Ordovician), Ohio and Kentucky. Journal of Sedimentary Petrology
63, 183–203. Doi: 10.1306/D4267ABE-2B26-11D7-8648000102C1865D

Jin, J., Harper, D.A.T., Cocks, L.R.M., McCausland, P.J.A., Rasmussen, C.M.Ø., Sheehan, P.M., 2013.
Precisely locating the Ordovician equator in Laurentia. Geology 41, 107–110. Doi:
10.1130/G33688.1

Kidwell, S.M., 1986. Models for fossil concentrations: paleobiologic implications. Paleobiology 12, 6–24.
Doi: 10.1017/S0094837300002943

Kidwell, S.M., 1989. Stratigraphic condensation of marine transgressive records: origin of major shell
deposits in the Miocene of Maryland. The Journal of Geology 97, 1–24. Doi:
https://doi.org/10.1086/629278

Kidwell, S.M., Jablonski, D., 1983. Taphonomic feedback: Ecological consequences of shell
accumulations. In: Allison, P.A., Briggs, D.E.G. (Eds.), Taphonomy: Releasing Data Locked in
the Fossil Record, New York, Plenum Press, 195–248.

Komar, P.D., 1989. Physical processes of waves and currents and the formation of marine placers. CRC
Critical Reviews in Aquatic Sciences 1, 393–423.

Kosik, N.P., Young, S.A., Bowman, C.N., Saltzman, M.R., Them, M.R., III. Middle-Upper Ordovician
(Darriwilian–Sandbian) paired carbon and sulfur isotope stratigraphy from the Appalachian
Basin, USA: Implications for dynamic redox conditions spanning the peak of the Great
Ordovician Biodiversification Event. Palaeogeography, Palaeoclimatology, Palaeoecology 520,
188–202.

Kruskal, W.H., Wallis, W.A., 1952. Use of ranks in one-criterion variance analysis. Journal of the
American Statistical Association 47, 260, 583–621.

Lucas, J., Prévôt, L.E., 1991. Phosphates and fossil preservation. In: Allison, P.A, Briggs, D.E.G. (Eds.), Taphonomy: Releasing the Data Locked in the Fossil Record, New York, Plenum Press, pp. 389–409.

Lucotte, M., Mucci, A., Hillaire-Marcel, C., and Tran, S., 1994. Early diagenetic processes in deep Labrador Sea sediments: reactive and nonreactive iron and phosphorus. Canadian Journal of Earth Sciences 31, 14–27. Doi: 10.1139/e94-003

Mac Niocaill, C., van der Pluijim, B.A., and Van der Voo, R., 1997. Ordovician paleogeography and the evolution of the Iapetus Ocean. Geology 25, 159–162.

Matthews, S.C., Missarzhevsky, V.V., 1975. Small shelly fossils of late Precambrian and early Cambrian age; a review of recent work. Journal of the Geological Society 131, 289–304. Doi: 10.1144/gsjgs.131.3.0289

McLaughlin, P.I., Brett, C.E., 2004. Eustatic and tectonic control on the distribution of marine seismites: examples from the Upper Ordovician of Kentucky, USA. Sedimentary Geology 168, 165–192. Doi: 10.1016/j.sedgeo.2004.02.005

Miller, A.I., 1997. Counting fossil in a Cincinnatian storm bed: spatial resolution in the fossil record. In: Brett, C.E., Baird, G.C. (Eds.), Paleontological Events: Stratigraphic, Ecological, and Evolutionary Implications. Columbia University Press, New York, pp. 57–72.

Miller, A.I., Holland, S.M., Meyer, D.L., Dattilo, B.F., 2001. The use of faunal gradient analysis for interregional correlation and assessment of changes in sea-floor topography in the type Cincinnatian. Journal of Geology 109, 603–613. Doi: https://doi.org/10.1086/321965

Mullins, H.T., Rasch, R.F., 1985. Sea-floor phosphorites along the Central California continental margin. Economic Geology 80, 696–715. Doi: 10.2113/gsecongeo.80.3.696

O'Brien, G.W., Milnes, A.R., Veeh, H.H., Heggie, D.T., Riggs, S.R., Cullen, D.J., Marshall, J.F., Cook, P.J., 1990. Sedimentation dynamics and redox iron-cycling: controlling factors for apatite-glauconite association on the east Australian continental margin. In: Notholt, A.J.G., Jarvis, I. (Eds.). Phosphorite Research and Development. Geological Society Special Publication 52, 61–86.

Pang, Y., Steiner, M., Shen, C., Feng, M., Lin, L., Liu, D., 2017. Shell composition of Terreneuvian tubular fossils from north-east Sichuan, China. Palaeontology 60, 15–26. Doi: 10.1111/pala.12268

Paytan, A., McLaughlin, K., 2007. The oceanic phosphorus cycle. Chemical Reviews 107, 563–576. DOI: 10.1021/cr0503613

Pojeta. J., Jr. 1979. (Ed.) Contributions to the Ordovician Paleontology of Kentucky and Nearby States. United States Geological Survey Professional Paper 1066-A–G.

Porter, S.M., 2004. Closing the phosphatization window: testing for the influence of taphonomic megabias on the pattern of small shelly decline. PALAIOS 18, 178–183. Doi: 10.1669/0883-1351(2004)019<0178:CTPWTF>2.0.CO;2

Poulton, S.W., Canfield, D.E., 2006. Co-diagenesis of iron and phosphorus in hydrothermal sediments from the southern East Pacific Rise: implications for the evaluation of paleoseawater phosphate concentrations. Geochimica and Cosmochimica Acta 70, 5883–5898. doi:10/1016/j.gca.2006.01.030.

Powell, E.N., Hu, X., Cai, W.-J., Ashton-Alcox, K.A., Parsons-Hubbard, K.M., Walker, S.E., 2012. Geochemical controls on carbonate shell taphonomy in northern Gulf of Mexico continental shelf and slope sediments. PALAIOS 27, 571–584. Doi: 10.2110/palo.2011.p11-116r

Pruss, S.B., Tosca, N.J., Stark, C., 2018. Small shelly fossil preservation and the role of early diagenetic redox in the Early Triassic. PALAIOS 33, 441–450. Doi: 10.2110/palo.2018.004

Pufahl, P.K., Grimm, K.A., Abdulkader, A.M., Sadaqah, R.M.Y., 2003. Upper Cretaceous (Campanian) phosphorites in Jordan: implications for the formation of a south Tethyan phosphorite giant. Sedimentary Geology 161, 175–205. Doi: 10.1016/S0037-0738(03)00070-8

Rasmussen, C.M.Ø., Kröger, B., Nielsen, M.L., Colmenar, J., 2019. Cascading trends of Early Paleozoic marine radiations paused by Late Ordovician extinctions, PNAS 116, 15, 7207–7213.

Servais, T., Harper, D.A.T., 2018. The Great Ordovician Biodiversification Event (GOBE): definition, concept, and duration. Lethaia 51, 151–164. Doi: 10.1111/let.12259

Schutter, S.R., 1996. The Glenwood Shale as an example of a Middle Ordovician condensed section. In: Witzke, B.J., Ludvigson, G.A., Day, J. (Eds.), Paleozoic Sequence Stratigraphy: Views from the North American Craton. Geological Society of America Special Paper 306, 55–65.

Scotford, D.M., 1965. Petrology of the Cincinnatian Series shales and environmental implications. Geological Society of America Bulletin 76, 193–222. DOI: 10.1130/0016-7606(1965)76[193:POTCSS]2.0.CO;2

Shaffer, G., 1986. Phosphate pumps and shuttles in the Black Sea. Nature 321, 515–517. Doi: 10.1038/321515a0.

Shvetsov, M.S., 1954. .Concerning some additional aids in studying sedimentary formations. Bulletin of the Moscow Society of Naturalists (Byulleten Moskovskogo Obscchestva Ispytateley Prirody), Publications of Moscow University, Geology Section 29(1), 61–66. (In Russian.)

Smosna, R., 1989. Compositional maturity of limestones—a review. Sedimentary Geology 51, 137–146. Doi: 10.1016/0037-0738(87)90044-3

Spearman, C. 1904. The proof and measurement of association between two things. American Journal of Psychology 15, 72–101. doi:10.2307/1412159.

Stigall, A.L., Edwards, C.T., Freeman, R.L., Rasmussen, C.M.Ø., this volume. Coordinated biotic and abiotic change during the Great Ordovician Biodiversification Event: Darriwilian assembly of Early Paleozoic building blocks. Palaeogeography, Palaeoclimatology, Palaeoecology.

Swanson-Hysell, N.L., Macdonald, F.A., 2017. Tropical weathering of the Taconic orogeny as a driver for Ordovician cooling. Geology 45, 719–722.

Terry R.D., Chiligar, G.V, 1955. Summary of "Concerning some additional aids in studying sedimentary formations" by M.S. Shvetsov. Journal of Sedimentary Petrology 25, 229-234. Doi: 10.1306/74D70466-2B21-11D7-8648000102C1865D

Tobin, R.C., 1982. A Model for Cyclic Deposition in the Cincinnatian Series of Southwestern Ohio, Northern Kentucky, and Southeastern Indiana. Ph.D. Dissertation, University of Cincinnati, Cincinnati, Ohio.

Tomašových, A., Kidwell, S.M., Barber, R.F., Kaufman, D.S., 2014. Long-term accumulation of carbonate shells reflects a 100-fold drop in loss rate. Geology 42, 819–822. Doi: 10.1130/G35694.1

Trappe, J., 1998. Phanerozoic Phosphorite Depositional Systems. Lectures Notes in Earth Sciences: Springer, Berlin.

Vendrasco, M.J., Checa, A., Heimbrock, W.P., Baumann, S.D.J., 2013. Nacre in molluscs from the Ordovician of the midwestern United States. Geosciences 3, 1–29. Doi: 10.3390/geosciences3010001

Vogel, K., Brett, C.E., 2009. Record of microendoliths in different facies of the Upper Ordovician in the Cincinnati Arch region, USA; the early history of light-related microendolithic zonation.

Palaeogeography, Palaeoclimatology, Palaeoecology 281, 1–24. Doi:

10.1016/j.palaeo.2009.06.032

Walter, L.M., Morse, J.W., 1984. Reactive surface area of skeletal carbonates during dissolution: effect of

grain size. Journal of Sedimentary Petrology 54, 1081–1090. Doi: 10.1306/212F8562-2B24-

11D7-8648000102C1865D

Webby, B.D., Paris, F., Droser, M.L., Percival, I.G., (Eds.), 2004. The Great Ordovician

Biodiversification Event. Columbia University Press, New York, 496 pp.

Webber, A.J., 2002. High-resolution faunal gradient analysis and an assessment of the causes of meter-

scale cyclity in the type Cincinnatian Series (Upper Ordovician). PALAIOS 17, 545–555. Doi:

10.1669/0883-1351(2002)017%3C0545:HRFGAA%3E2.0.CO;2

Witzke, B.J., 1987. Models for circulation patterns in epicontinental seas applied to Paleozoic facies of

North America craton. Paleoceanography 2, 229–248.

Witzke, B.J., Heathcote, R.C., 1997. Lower Maquoketa phosphatic and organic-rich facies, Upper

Ordovician, Dubuque County. Geological Society of Iowa Guidebook 63, 25–37.

Young, S.A., Saltzman, M.R., Foland, K.A., Linder, J.S., Kump, L.R., 2009. A major drop in seawater

87Sr/86Sr during the Middle Ordovician (Darriwilian): links to volcanism and climate. Geology

37, 951–954. Doi: /10.1130/G30152A.1

Zuschin, M., Stachowitsch, M., Stanton, R.J., Jr., 2003. Patterns and processes of shell fragmentation in

modern and ancient marine environments. Earth-Science Reviews 63, 33–82. Doi: